Thesis for the Degree of Licentiate of Engineering

Active Transmitter Antenna Array Modeling for MIMO Applications

Parastoo Taghikhani

CHALMERS

Chalmers University of Technology
Department of Microtechnology and Nanoscience (MC2)

Göteborg, Sweden 2020

Active Transmitter Antenna Array Modeling for MIMO Applications

Parastoo Taghikhani

© Parastoo Taghikhani, 2020.

Technical report number: MC2-431
ISSN 1652-0769

Chalmers University of Technology
Department of Microtechnology and Nanoscience (MC2)
Microwave Electronics Laboratory
SE–412 96 Göteborg
Sweden
Telephone: +46 (0)31 – 772 1000
Email: parastoo@chalmers.se; parastoo.taghikhani@gmail.com

Typeset by the author using LaTeX.

Chalmers Reproservice
Göteborg, Sweden 2020

To my family

Abstract

The rapid growth of data traffic in mobile communications has attracted interests to the Multiple-Input-Multiple-Output (MIMO) communication systems at millimeter-wave (mmWave) frequencies. MIMO systems exploit active transmitter antenna arrays for higher energy efficiency and providing beamforming flexibility. The close integration of multiple PAs and antennas increases the transmitter analysis complexity. Moreover, due to the small antenna element spacing at mm-wave frequencies, isolators are too bulky and cannot be used. Therefore, including the effects of interactions between the antenna array and PAs is a significant aspect in the analysis of MIMO transmitters. For large active arrays, applying joint circuit and EM simulation tools for the analysis is a complicated and time-consuming task. In these occasions, behavioral models are the key to the fast and accurate evaluation of active transmitter antenna arrays.

In this thesis, a technique for modeling the active transmitter antenna array performance is presented. The proposed model considers the effect of PAs nonlinearity as well as the coupling and mismatch in the antenna array. With this model, a comprehensive prediction of radiation pattern and signal distortions in the far-field is feasible. The model is experimentally verified by a mmWave active subarray antenna for a beam steering scenario and by performing over-the-air measurements. The measurement results effectively validate the modeling technique for a wide range of steering angles.

Furthermore, a linearity analysis is provided to predict transmitter performance in conjunction with beam-dependent digital predistortion (DPD) linearization. The study reveals the model potential in evaluating different DPD approaches as well as predicting the performance of linearized transmitters. The demonstration shows that the variation of nonlinear distortion versus steering angle depends significantly on the array configuration and beam direction.

In summary, the proposed model allows for the prediction of the active transmitter antenna array performance in the early design stages with low computational effort. It can provide design guides for developing large-scale active arrays and can be employed for evaluating the DPD and transmitter linearity performance.

Keywords: Active antenna array, active impedance, beam steering, far-field nonlinear distortion, hybrid beamforming transmitter, millimeter wave, MIMO transmitter, modeling.

Acknowledgments

I have received the help and company of many people during my doctoral study and I here would like to recognize their invaluable assistance.

First, I would like to express my deepest gratitude to my main supervisor, Professor Christian Fager for guidance, encouragement, and patience. Thank you for the trust and confidence that you have shown in me, which helped me to work to the best of my ability. Without your continuous and comprehensive support, I couldn't pursue my challenging project.

I would also like to extend my sincere thanks to my co-supervisor Assistant Professor Koen Buisman for ingenious advice and feedback on my research. Thank you for always being supportive and committed to my work. I wish to express my appreciation to my examiner Professor Herbert Zirath. It is a great honor for me to be part of your inspiring research group. Special thanks go to all the colleagues of the Microwave Electronics Laboratory for the supportive and friendly work environment. I also gratefully acknowledge the assistance of our collaborators from Antenna Research Group, Professor Marianna Ivashina and Associate Professor Rob Maaskant.

I would like to thank NXP Semiconductor for hosting my eighteen-months industrial internship. In particular, I wish to thank Ir. Marcel Geurts for the productive collaboration and hospitality at NXP. I also wish to thank Ir. Martin Versleijen, my industrial supervisor, for the guidance and patience that cannot be underestimated. I am very grateful for everything you thought me.

I have had the chance to enjoy the company of many friends from Chalmers university, SILIKA project, and NXP semiconductor company in these years. I wish to thank all of them for cheering me up and for their reliable friendship.

And finally, thank to Abolfazl, who has been by my side throughout these years, living every single minute of it, and without whom, I would not have proceeded to this stage.

Parastoo
Göteborg, May 2020

List of Publications

This thesis is based on the following appended paper:

Paper A
P. Taghikhani, K. Buisman and C. Fager, "Hybrid Beamforming Transmitter Modeling for Millimeter-Wave MIMO Applications", Accepted for publication in *IEEE Transactions on Microwave Theory and Techniques, April, 2020.*

Other related publications by the Author not included in this thesis:

[i] M. SalarRahimi, E. V. P. d. Anjos, **P. Taghikhani**, V. Volski, C. Fager, D. M. M. Schreurs , G. A. E. Vandenbosch, M. Geurts "A Cost-Efficient 28 GHz Integrated Antenna Array with Full Impedance Matrix Characterization for 5G NR", *IEEE Antennas and Wireless Propagation Letters*, vol. 19, no. 4, pp. 666-670, April 2020.

[ii] H. V. Hünerli, M. Gavell, **P. Taghikhani** and C. Fager, "A Methodology for Analysis of mm-Wave Transmitter Linearization Trade-offs Under Spectrum Constraints", *2018 International Workshop on Integrated Nonlinear Microwave and Millimetre-wave Circuits (INMMIC)*, Brive La Gaillarde, 2018, pp. 1-3.

[iii] J. Yang, F. Fangfang and **P. Taghikhani**, "Half-height-pin Gap Waveguide Technology and its Applications in High Gain Planar Array Antennas at MillimeterWave Frequency", *IEICE Transactions on Communications*, vol. 101, no. 2, pp. 285-292, 2018.

[iv] **P. Taghikhani**, J. Yang and A. Vosoogh "High gain V-band planar array antenna using half-height pin gap waveguide,", *2017 11th European Conference on Antennas and Propagation (EUCAP)*, Paris, 2017, pp. 2758-2761.

Acronyms

AMAM	Amplitude Modulation to Amplitude Modulation
AMPM	Amplitude Modulation to Phase Modulation
CAD	Computer Aided Design
CW	Continous Wave
DPD	Digital Predistortion
EM	Electromagnetic
FIR	Finite Impulse Response
IC	Integrated Circuit
LTE	Long Term Evolution
MIMO	Multiple-Input Multiple-Output
mmWave	Millimeter Wave
OTA	Over The Air
PA	Power Amplifier
PAPR	Peak to Average Power Ratio
PHD	Poly Harmonic Distortion
RF	Radio Frequency
RX	Reciever
TX	Transmitter
VNA	Vector Network Analyzer

Contents

Chapter 1

Introduction

1.1 Background

Nowadays, people, societies, and organizations demand faster and more reliable communications. The number of fixed and mobile communication devices are inevitably increasing per year. An estimate by Ericsson [1] shows that the number of mobile subscriptions will be around 8 billion at the end of 2025. Among the different generations of radio networks, 5th Generation (5G) is expected to serve around 2.6 billion mobile subscribers and be the fastest deployed mobile communication in history [1]. Fig. 1.1 shows the anticipated growth of mobile and fixed subscription until 2025 [1].

The main spectrum options for 5G in its early phases is sub-6 GHz. However, the available bandwidth at sub-6 GHz is not enough to meet the anticipated capacity demands for the 5G era. Therefore, as a complement to the current sub-6 GHz, vast available bandwidth at mmWave bands, frequencies between 24 and 71 GHz, is opened up for 5G communications [1–5]. The benefit of mmWave usage comes at the price of higher propagation loss. According to the Friis transmission formula, the path loss increases proportionally to λ^{-2} (λ is wavelength). [6]. However, the mmWave loss can be partially compensated by using high gain antennas or large-scale antenna arrays. Particularly, the use of antenna arrays provides beamforming flexibility, which is also highly favorable for massive Multiple Input Multiple Output (MIMO) mobile communications. Therefore, the use of large antenna arrays are beneficial for increasing signal strength toward the user, overcome path loss, and higher capacity of MIMO communication [7, 8].

To obtain the most flexibility of beamforming, it is favorable to have an independent TX/RX RF chain per antenna. This configuration is referred to as a digital beamforming architecture. Due to complexity and higher power consumption of a fully digital architecture, there is a growing interest in implementing hybrid digital and analog architectures for mmWave MIMO

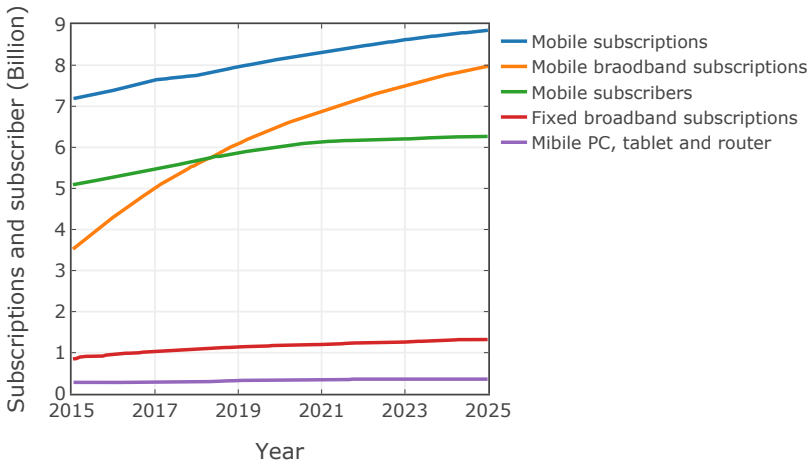

Figure 1.1: Anticipated number of mobile and fixed subscriptions and subscribers (billions) until 2025 [1].

systems. In hybrid architectures, each RF chain is connected to a subarray of antennas with an analog beamforming network [9–11]. The number of users that can be served simultaneously with hybrid structures is thereby limited to the number of dedicated RF chains. Fig. 1.2 shows the transmitter of a MIMO system with digital and hybrid beamforming architectures. Both architectures employ the active antenna array in which each antenna element is driven by a power amplifier (PA). Traditionally, for an active array, isolators have been used to eliminate mismatch and unwanted interactions between PAs and antennas. However, due to the small antenna element spacing at mmWave frequencies, isolators are too bulky and cannot typically be used. Therefore, PAs are susceptible to the coming waves from the antenna array due to mismatch and mutual coupling between antenna elements. In this condition, including the effects of interactions between the antenna array and PAs becomes a significant aspect in the analysis of an active transmitter antenna array.

An accurate prediction of the transmitter performance is crucial in the early design stage. Particularly, with the aid of an accurate performance analysis, applying necessary modifications before implementing the transmitter is feasible. It can be also used for evaluating the compensation techniques such as Digital pre-distortion (DPD).

Dedicated electromagnetic (EM) and circuit computer aided design (CAD) simulation tools are available for the design and analysis of antenna array and PAs individually. However, such a detailed simulation is not

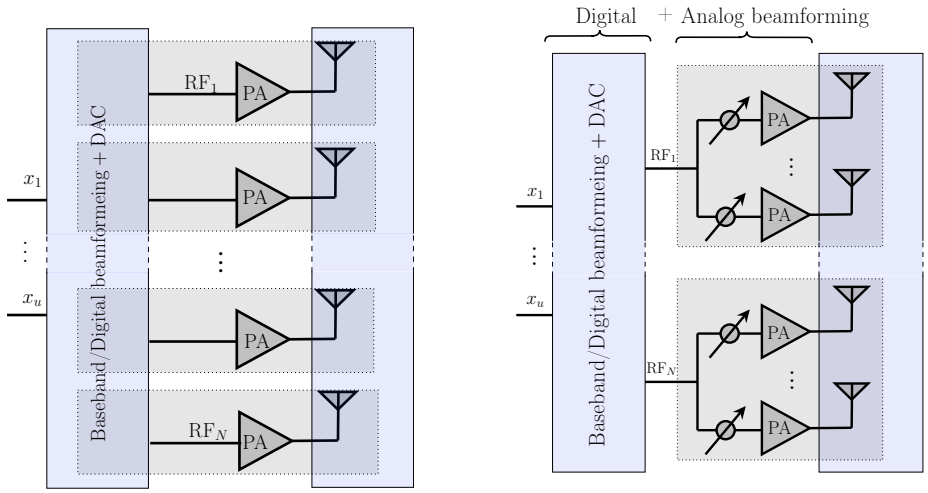

Figure 1.2: Different architectures for a transmitter in a MIMO system. a) Digital beamforming, b) Hybrid digital and analog beamforming architecture.

suitable for understanding the behavior at transmitters level. Moreover, applying joint circuit and EM simulation tools is a complicated and time-consuming task for the analysis of large active arrays. In these occasions, an analysis approach based on behavioral models of the PA and antenna array is the key to fast and accurate evaluation of active transmitter antenna arrays. These models can be obtained from CAD simulation tools or measurements and must adequately present the performances of the devices. Fig. 1.3 shows the generic analysis framework for the active transmitter antenna array including signal processing unit, antenna and PA models. The active transmitter antenna array in this framework is modeled by employing PA and antenna array models, and considering their interactions.

1.2 Thesis Scope

This thesis attempts to develop a modeling approach for active transmitter antenna arrays. The modeling approach addresses the joint PA and antenna effects on the antenna array performance such as radiation pattern and active input impedance. It also predicts the radiated signal characteristics such as in-beam nonlinearity and radiation pattern. The work of this thesis is intended to be applicable for both digital and hybrid beamforming transmitters. However, particular attention is paid to the hybrid beamforming architecture and beam steering scenarios to show the importance of considering joint PA and antenna effect in the transmitter analysis. To

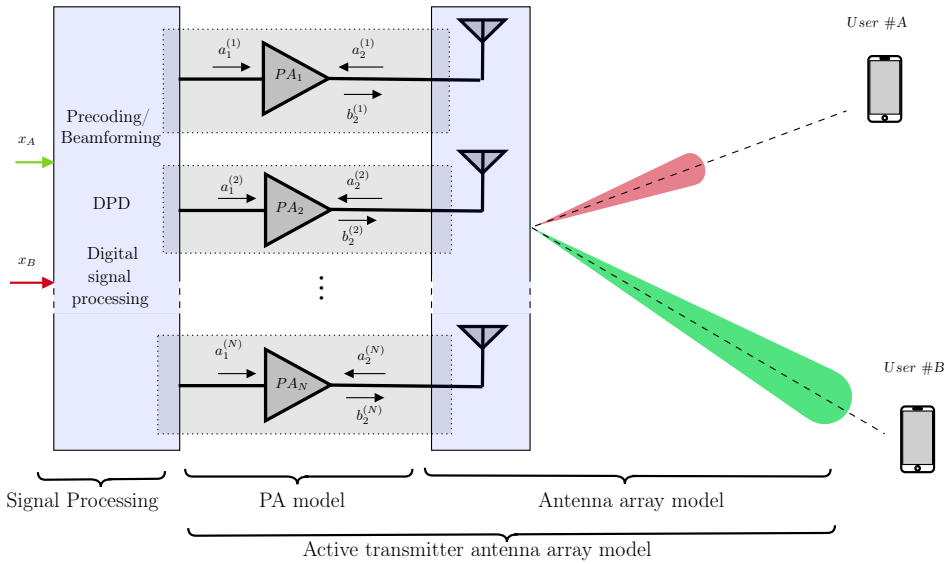

Figure 1.3: The analysis framework for an active transmitter antenna array.

validate the proposed analysis, we have performed experiments with a hybrid beamforming subarray module including a typical beamforming Integrated Circuits (IC) and a subarray antenna. The experimental validation results are therefore demonstrated for a beam steering scenario. The transmitter model is then exploited in a simulation study to predict the linearity of different array configurations.

1.3 Thesis Outline

This thesis is organized in five chapters. In chapter 2, the theoretical background of antenna arrays and its basic notation is provided. This explains the concept of array radiation pattern and beam steering/phased array in an antenna theory context. With the antenna array theory, the effect of antenna excitation variations i.e PA outputs, on the radiation pattern is better understood. Also, it will explain the concept of mutual coupling and embedded element patterns, which are crucial in the analysis of active transmitters with coupled antenna elements. In chapter 3, basic PA characteristics, and a variety of behavioral models are described. First, a brief introduction to PA fundamental nonlinear characteristic is given. Then, the nonlinear PA models for transmitters with isolated and coupled paths are described. In chapter 4 the active transmitter antenna array modeling approaches are investigated. The existing transmitter modeling techniques are reviewed and our proposed modeling technique is described. Chapter 5 provides the conclusion of the thesis, main contributions, and future work.

Chapter 2

Antenna Array Characteristics

An array of antennas is a set of multiple antennas that are working together. The antenna array is designed such that the combined radiated signal has desired characteristics [12]. MIMO arrays can be thought of as an antenna array with advanced adaptive beamforming/signal processing which exploits the complex surrounding environment to improve performance, e.g. in terms of channel capacity. Therefore, an antenna array can have a wide range of architectures and capabilities. However, the underlying operating principle is common among all configurations and applications.

The antenna elements and excitation network are the two main parts of every antenna array. The excitation network is responsible for exciting the antenna elements such that the desired radiation characteristics are obtained. The array is called passive when the feeding network excites antenna elements from a common path. The active array is referred to as an array where each antenna element has a dedicated transmit or receive feeding path [12]. The active antenna array is more flexible and powerful, especially for beamforming purposes.

This chapter introduces the basic theory of the antenna array. The objective is to describe the antenna array concept and more specifically beam steering/phased array antennas. First, the analysis of the classical form of an antenna array is described. Then the phased array antenna and beam steering concept is introduced. In the next part, the effect of mutual coupling on antenna array performance is discussed. The antenna element embedded pattern and active impedance are described for analyzing antenna arrays with mutual coupling.

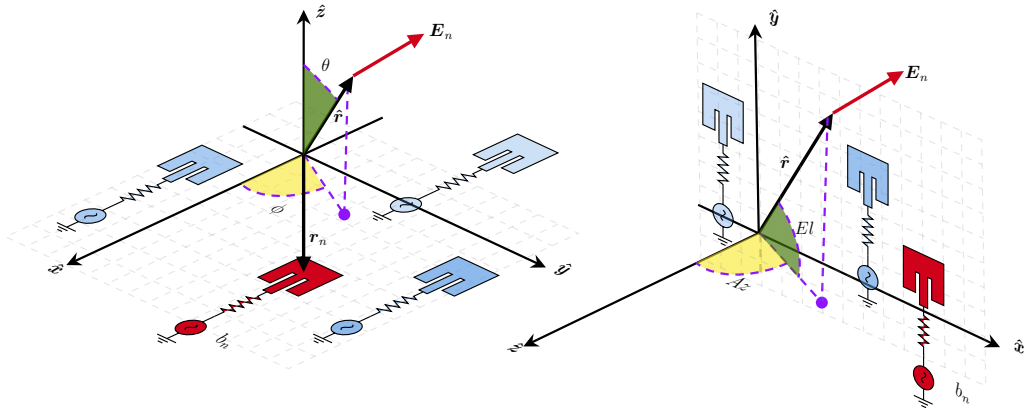

Figure 2.1: Illustration of a generic antenna array layout in spherical coordinate system (left) and Azimuth/Elevation coordinate system (right); each antenna element is located in position $\boldsymbol{r}_n$. The element radiated field is $\boldsymbol{E}_n$, and excitation waves are b_n.

2.1 Theory of Antenna Array

Consider N antenna elements that are located at $\boldsymbol{r}_n = x_n\hat{\boldsymbol{x}} + y_n\hat{\boldsymbol{y}} + z_n\hat{\boldsymbol{z}}, n = 1, 2, ..., N$. (x_n, y_n, z_n) is the location of n-th antenna element. $\hat{\boldsymbol{r}}(\theta, \phi) = \sin(\theta)\cos(\phi)\hat{\boldsymbol{x}} + \sin(\theta)\sin(\phi)\hat{\boldsymbol{y}} + \cos(\theta)\hat{\boldsymbol{z}}$ shows the vector of observation point at (θ, ϕ), see Fig. 2.1. $\boldsymbol{E}_n(\hat{r})$[1] is the element far-field radiation function[2] which is represented with respect to the array origin [12]. The radiation function, also defined as radiation pattern, represents the angular distribution of the radiated electric field of an antenna in the far-field region [13]. The radiation pattern is independent of the radial distance from the antenna in the far-field region. $\boldsymbol{E}(\hat{r})$ is the array radiation pattern and is calculated as

$$\boldsymbol{E}(\hat{\boldsymbol{r}}) = \sum_{n=1}^{N} b_n \boldsymbol{E}_n(\hat{\boldsymbol{r}}), \quad \text{with} \quad \boldsymbol{E}_n(\hat{\boldsymbol{r}}) = \boldsymbol{E}_n^o(\hat{\boldsymbol{r}}) e^{jk_0 \boldsymbol{r}_n \cdot \hat{\boldsymbol{r}}}. \tag{2.1}$$

$\boldsymbol{E}_n^o(\hat{\boldsymbol{r}})$ is the element radiation pattern where the origin is on the antenna element itself, and assuming that the incident input power to the antenna element is unitary. $k_0 = 2\pi/\lambda$ is the wavenumber and $b_n = A_n e^{j\phi_n}$ is the complex value of the incident power wave to the n-th element with incident input power equal to $P_n^{inc} = \frac{1}{2}|b_n|^2$.

As it can be seen in Fig. 2.1, the (θ, ϕ) in spherical coordinate system

[1] $\boldsymbol{E} = \boldsymbol{E}_n(\hat{r})$ is the electric field vector which in cartesian coordinate system can be written as $\boldsymbol{E} = E_x\hat{\boldsymbol{x}} + E_y\hat{\boldsymbol{y}} + E_z\hat{\boldsymbol{z}}$.

[2] Assuming the antenna elements are isolated. The accurate term is the embedded element radiation function which will be introduced in 2.3.

converts to (Az, El) angle by

$$\begin{aligned} \sin(El) &= \sin(\phi)\cos(\theta), \\ \tan(Az) &= \cos(\phi)\tan(\theta). \end{aligned} \tag{2.2}$$

(2.1) shows that the array radiation pattern depends on the individual element radiation patterns, positions and incident waves. The physical geometry of the array determines the first two quantities. However, the incident power waves are determined by the feeding network e.g. the PA outputs in an active antenna transmitter. It is common to assume that the antenna elements have equal radiation patterns. However, under mutual coupling this assumption is not true. If we assume all antenna elements have similar radiation pattern, $\boldsymbol{E}_0^o(\hat{\boldsymbol{r}})$, the array radiation pattern can be written as

$$\boldsymbol{E}(\hat{\boldsymbol{r}}) = \boldsymbol{E}_0^o(\hat{\boldsymbol{r}})F(\hat{\boldsymbol{r}}), \quad \text{with} \quad F(\hat{\boldsymbol{r}}) = \sum_{n=1}^{N} b_n e^{jk_0 \boldsymbol{r}_n \cdot \hat{\boldsymbol{r}}}, \tag{2.3}$$

where F is called array factor. The above expression is valid for antenna arrays where mutual coupling between elements can be ignored.

2.2 Phased Array and Beam Steering

Phased arrays are antenna arrays that can provide electronic beam steering. Electronic beam steering is performed by applying phase-shifted excitations to the antenna elements. The beam steering allows pointing the beam toward specific users for tracking or sweeping a large spatial sector quickly [14]. However, to have a highly directive beam at a specific steer direction, it is important to design antenna element and array layout properly. Consider the $\hat{\boldsymbol{r}}_s$ is supposed to be the steer direction. By applying the incident waves according to $b_n^s = A_n e^{-jk_0 \boldsymbol{r}_n \cdot \hat{\boldsymbol{r}}_s}$, the array factor represented in (2.3) is modified as:

$$F^s(\hat{\boldsymbol{r}}) = \sum_{n=1}^{N} b_n^s e^{jk\boldsymbol{r}_n \cdot \hat{\boldsymbol{r}}} = \sum_{n=1}^{N} A_n e^{jk\boldsymbol{r}_n \cdot (\hat{\boldsymbol{r}} - \hat{\boldsymbol{r}}_s)}. \tag{2.4}$$

(2.4) shows that, at the direction $\hat{\boldsymbol{r}} = \hat{\boldsymbol{r}}_s$, the array factor and consequently the radiation function is maximum[3].

Consider a linear array in which elements are located along the x-axis. The inter-element spacing is d, and the number of elements is N. Fig. 2.2

[3]If the antenna element radiation function is not relatively low at $\hat{\boldsymbol{r}} = \hat{\boldsymbol{r}}_s$.

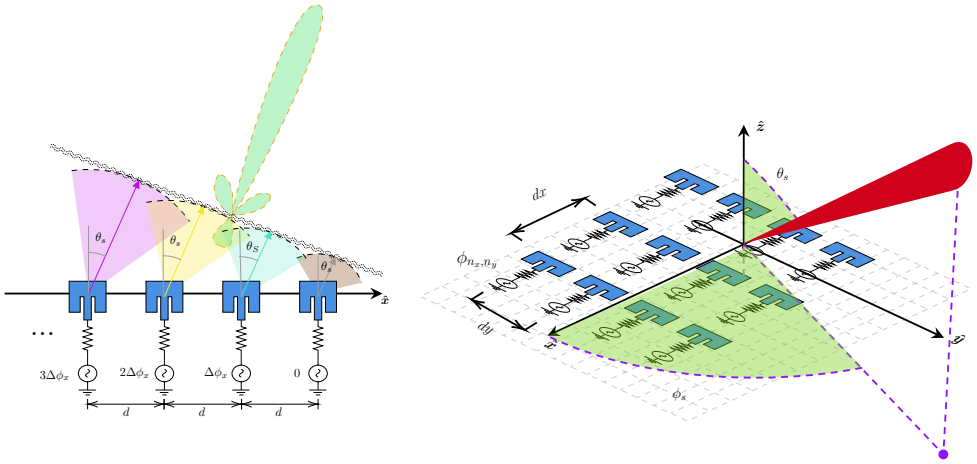

Figure 2.2: Illustration of a linear (left) and planar (right) phased array; $\Delta\phi_x$ is phase shift in linear array. N_x and N_y are the number of elements in planar array along x and y axis, respectively. ϕ_{n_x,n_y} is the excitation phase of corresponding element.

shows the configuration of the linear phased array and its radiation pattern. Based on the above explanation, the incident waves for steering the beam to θ_s is

$$b_n^s = A_n e^{jk\boldsymbol{r}_n\cdot\hat{\boldsymbol{r}}_s}, \quad \text{with} \quad \hat{\boldsymbol{r}}_s = \hat{\boldsymbol{x}}\sin(\theta_s) + \hat{\boldsymbol{z}}\cos(\theta_s), \quad \boldsymbol{r}_n = nd\hat{\boldsymbol{x}}. \tag{2.5}$$

Therefore, for an equally spaced linear array the phase shifting between element along the x-axis is obtained as:

$$\Delta\phi_x = kd\sin(\theta_s). \tag{2.6}$$

The phase-shifting of the equally spaced planar array can be easily found using a similar approach. Consider a planar array with element spacing as d_x and d_y for the elements along the x- and y-axis. (n_x, n_y) with $n_x = 1, ..., N_x$ and $n_y = 1, ..., N_y$ shows the element index. To steer the antenna array beam toward (ϕ_s, θ_s), the phase-shifting between elements along the x- and y-axis are obtained as

$$\begin{aligned}\Delta\phi_x &= kd_x\sin(\theta_s)\cos(\phi_s),\\ \Delta\phi_y &= kd_y\sin(\theta_s)\sin(\phi_s).\end{aligned} \tag{2.7}$$

Therefore, the excitation phase of element (n_x, n_y) is

$$\phi_{n_x,n_y} = -n_x\Delta\phi_x - n_y\Delta\phi_y. \tag{2.8}$$

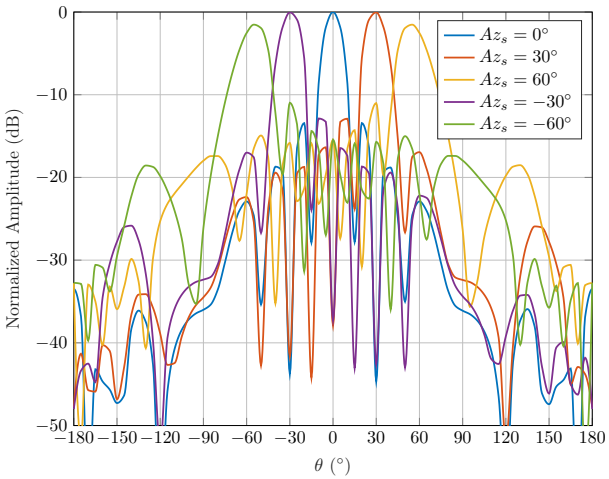

Figure 2.3: Radiation pattern of an 8×8 microstrip patch antenna array in the $El_s = 0$ (x-z) plane. The steer angles are $El_s = 0$; $Az_s = -60°, -30°, 0°, 30°, 60°$.

As an example, Fig. 2.3 shows the radiation pattern of a 29 GHz 8×8 microstrip patch antenna array, with 0.5λ element spacing along x and y directions for different steer angles.

2.3 Effect of Mutual Coupling

Every antenna element is typically characterized in isolation and away from surrounding bodies. In an array, the antenna element radiation characteristics are strongly affected by the neighboring antennas. The proximity between antenna elements can strongly change the far-field radiation pattern and impedance characteristics of each element. These effects are referred to as mutual coupling and are often undesired in antenna arrays. For weakly coupled antennas, it is common to assume identical and isolated element radiation patterns. In a dense array, element radiation patterns can be very different from one another. Exciting one antenna element induces a current in the neighboring elements. The neighboring element thereby re-radiate and subsequently couples to the other antennas. Therefore, the total radiation pattern due to the radiation of induced current changes. Also, the induced coupled current to the nearby antenna changes its port impedance. These effects are dependent on the antenna element excitations and the mutual coupling level. For an antenna array, the terms embedded element pattern and active impedance are defined to represent radiation pattern and port impedance in presence of mutual coupling.

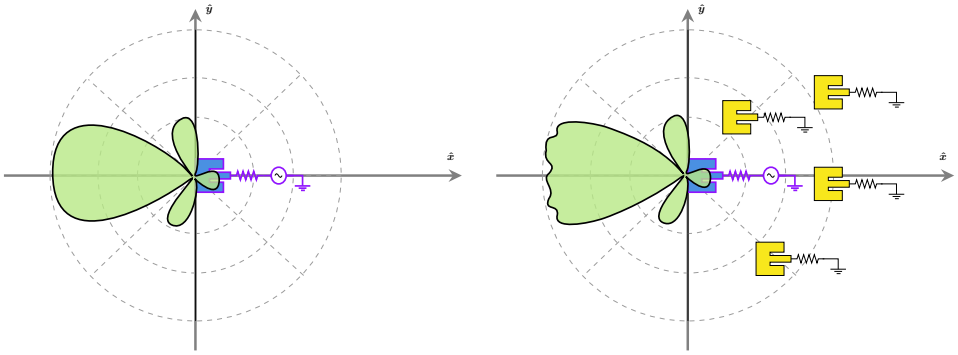

(a) (b)

Figure 2.4: The antenna element radiation pattern. a) Isolated element pattern, b) Embedded element pattern; For a weakly coupled array, the isolated element pattern and embedded element pattern become similar.

2.3.1 Embedded element pattern

The embedded element pattern is defined as the array radiation pattern when one element is excited and the rest of the elements are passively terminated by a matched load, see Fig. 2.4 (b). (2.1) then can be adopted based on embedded element patterns. In this representation, the mutual coupling effects are incorporated in the embedded element pattern definition and consequently into the antenna array radiation pattern [15]:

$$\boldsymbol{E}(\hat{\boldsymbol{r}}) = \sum_{n=1}^{N} b_n \boldsymbol{E}_n^{em}(\hat{\boldsymbol{r}}). \tag{2.9}$$

In this formulation, it is assumed that embedded element radiation pattern is represented in respect to the antenna array origin. Otherwise, the $\boldsymbol{E}_n^{em}(\hat{\boldsymbol{r}})$ must be modified accordingly.

2.3.2 Active impedance

Each antenna element is characterized solely by its self-impedance. However, when an antenna element is placed in an array configuration its input impedance changes due to mutual coupling. The term active impedance refers to the input impedance of an element when all other array elements are active or excited. The active impedance varies with array element excitations and mutual coupling [15, 16]. Therefore, for a phased array it depends on the steering angle. In principle, the active impedance is different for each antenna element inside the array. For an array of N elements, the S-parameter is an $N \times N$ matrix which includes mismatch and mutual

coupling of the array. $\boldsymbol{s}_{n,m}$ are the elements of the array S-parameter matrix. Considering that the element excitations, b_n, are known, the i-th element active reflection coefficient is calculated as

$$\Gamma_i^{\text{act}} = \frac{\sum_{n=1}^{N} b_n \boldsymbol{s}_{n,m}}{b_i}, \tag{2.10}$$

and accordingly, the active impedance with reference to Z_0 is

$$Z_{\text{act},i} = Z_0 \frac{1+\Gamma_i}{1-\Gamma_i}. \tag{2.11}$$

$Z_{\text{act},i}$ is the antenna port impedance when all other antenna elements of the array are active.

2.4 Summary

In this chapter, the theoretical background on antenna arrays is briefly given. First, the fundamental basics and terminology of antenna arrays radiation patterns are introduced. Then, a short introduction to the phased array is presented. Phased arrays were presented as a solution for beam steering to track and maximize energy direct to a user. Finally, the effect of mutual coupling on the antenna port impedance and the array radiation pattern is presented.

The analysis of antenna arrays is a well-established topic in the antenna research area. A variety of EM simulation tools such as CST Microwave studio and Ansys HFSS are available for highly accurate simulation of antenna and post-processing of antenna arrays. To analyze large-scale transmitter performance, a model which adequately represents antenna array behavior is applied.

Chapter 3

Power Amplifier Modeling

Power amplifiers (PA) play an important role in a wireless communication systems. The PA principle role is to amplify the signal to be at a suitable power level for transmission. However, PAs are a major contributor to the power consumption, signal distortion, and efficiency of the transmitter [17]. To analyze active transmitter antenna array performance, it is critical to characterize PA behavior properly.

A PA behavioral model is intended to characterize the PA behavior such as output power, efficiency, etc. as a function of different input variables [18]. To create a behavioral model, it is required to define the model structure, collect a set of input and output data, and determine model parameters. The model applicability depends on the model structure. An example could be static and dynamic models that are developed for the correct prediction of a single tone or wideband input signals. A variety of PA behavioral models have been proposed so far for different applications. PA models can be categorized as single input models and load-dependent models. The latter have been proposed for MIMO systems where the PA output is subject to signals coming from other transmit branches.

This chapter presents a brief introduction to the PA nonlinear characteristics, modeling structures, and model identification. The first section describes important PA characteristics. Then single input and dual input PA models are introduced in Sec. 3.2 and Sec. 3.3, respectively. Finally, techniques for model identifications are described and the chapter ends with a summary.

3.1 AM/AM and AM/PM Characteristics

Power amplifiers are commonly characterized by their gain and phase-shift as a function of inputs, or output power. These characteristics are called

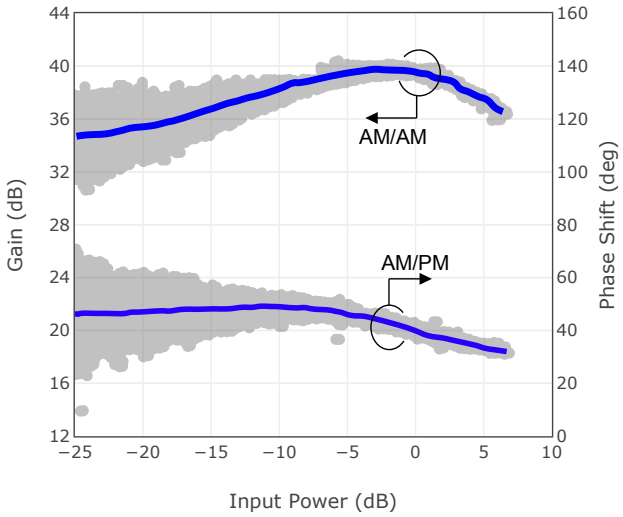

Figure 3.1: An example of PA AM/AM and AM/PM characteristics. Dispersive gray dots show dynamic PA behavior under modulated input signal with 10 MHz bandwidth [20].

amplitude modulation to amplitude modulation (AM/AM) and amplitude modulation to phase modulation (AM/PM). The shape of the AM/AM and AM/PM curves provide insightful information about the PA nonlinearities [19]. Typically, AM/AM and AM/PM characteristics are obtained when a PA is excited with a single tone signal. In this case, the AM/AM and AM/PM curve are a one to one mapping. Under modulated signal excitation, the instantaneous gain and output phase versus instantaneous input power is plotted to show dynamic AM/AM and AM/PM characteristics. Therefore, these curves show dispersive data. The dispersion gives a qualitative indication of the PA memory effects. Fig. 3.1 represents the measured AM/AM and AM/PM of a class AB PA which is operated at 2 GHz [20].

3.1.1 Memory effect

The PA distortion behavior can be divided into static, or memoryless, and dynamic categories. Generally, PAs are classified as nonlinear systems with memory. By definition, the output of a system with memory at any instant is not only a function of corresponding input but also depends on inputs at other past instants. The memory effect is an inherent characteristic of a power amplifier. The PA intrinsic, and extrinsic parasitic elements, reactive element in matching network, and the transistor junctions are energy

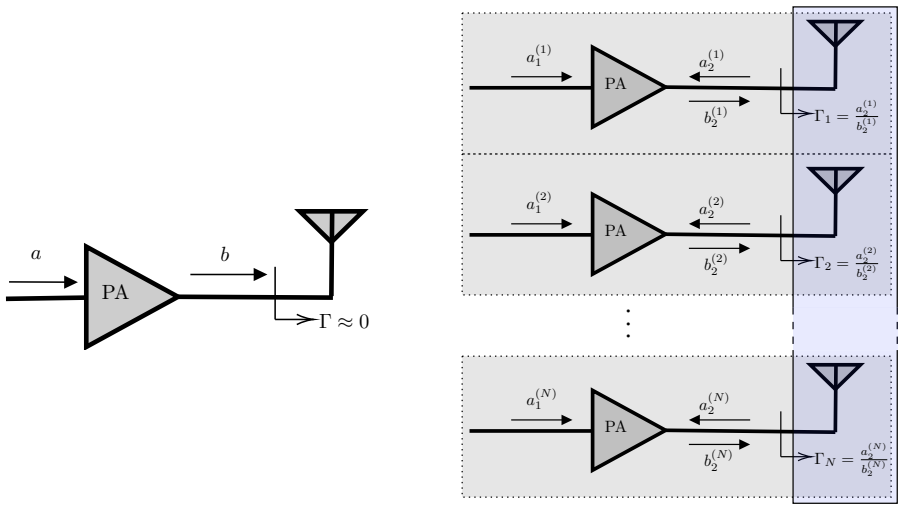

(a) (b)

Figure 3.2: Block diagram of a) single path, b) multi path transmitter for the purpose of PA modeling

storage parts of the PA circuit which cause memory effects. Self-heating is also another key source of memory effects in PAs [21]. However, for applications where the input signal is a single tone or a modulated signal with relatively narrow bandwidth, the memory effects of the PA can be neglected. This simplification is valid if the amplifier behavior is constant/flat over the bandwidth of the input signal. In this case, AM/AM and AM/PM conversion of PA at the carrier frequency characterize the PA within the signal bandwidth [19].

3.2 Single Input PA Model

The transmitter in a traditional wireless communication system includes one transmit path. Fig. 3.2(a) shows the block diagram of a single path transmitter for PA modeling. The power wave terminology is used to describe PA input and output. The usage of isolators and 50 Ω matching interfaces between different components ensure one directional signal flow from input to output. Therefore, the reflected wave in the opposite direction can be ignored. Most of the published PA behavioral models are given in complex baseband envelope descriptions [22]. Therefore, here we use similar notation in which the incident and reflected power waves to the PA are presented in the complex baseband envelop form.

The structure of a suitable PA behavioral model for the analysis of a

single-chain transmitter is presented as

$$b(n) = f(a(n)), \tag{3.1}$$

where $b(n)$ is the PA output power wave and described as a function of the power wave incident to the PA input $a(n)$. The function f, characterizes PA nonlinear behavior. Moreover, for simplicity in mathematical representation, the dependency of $b(n)$ to current and past samples of input waves, i.e. $f(a(n-1), a(n-2), ...)$ is not shown here and throughout the thesis. Such a model is also valid for the multi-antenna transmitters if the RF paths are isolated from each other.

Finding a suitable model structure has been an important research topic. Many different types of functions have been proposed for the single input PA model structure [23–26]. Volterra series model and the pruned version of it i.e. polynomial, memory polynomial [25], generalized memory polynomial [26] are among the most popular PA behavioral models. As an example, we introduce a polynomial and a memory polynomial model. The polynomial model, which is relevant for representing PAs with static behavior is represented as

$$b(n) = \sum_{p=0}^{(P-1)/2} c_p a(n)|a(n)|^{2p}, \tag{3.2}$$

where $b(n)$ and $a(n)$ are the baseband complex envelop of PA input and output power waves. c_p are the complex model coefficients and P is the nonlinear model order. Only odd-order terms are present since the distortions produced by the even-order components are far from the carrier frequency and do not contribute to the PA output within its intended bandwidth [27].

The memory polynomial model for characterizing PAs with dynamic behavior is formulated as

$$b(n) = \sum_{p=0}^{(P-1)/2} \sum_{m=0}^{M} c_{pm} a(n-m)|a(n-m)|^{2p}, \tag{3.3}$$

where c_{mp} are the model complex coefficients. P and M represent the nonlinear model order and memory depth, respectively.

The presented models in (3.2) and (3.3) are linear in the coefficients. Therefore, a least square solution can be used to estimate the model coefficients. The detailed description of the least square estimator is described in Sec. 3.4.2.

3.3 Dual Input PA Model

The transmitter in MIMO systems uses several RF transmit chains, each of them including individual PAs to drive an antenna array. In modern transmitters, bulky isolators between PA and antennas are avoided due to the high level of integration and lack of spacing. Therefore, PAs become susceptible to the waves leaking from other branches. Particularly, mismatch and mutual coupling in the antenna array create a variable active load, Γ_i, at the output of each PA, as described in Sec. 2.3. The variation in the impedance seen by each PA affects the linear and nonlinear behavior it exhibits. On these occasions, conventional PA models cannot perfectly describe their behavior. Fig. 3.2(b) presents the block diagram for modeling PA in a MIMO system. The PA output in k-th branch is described as

$$b_2(n) = f(a_1(n), a_2(n)), \tag{3.4}$$

where $b_2(n)$ is the PA output and described as a function of the two incident input power waves, i.e $a_1(n), a_2(n)$ in the k-th transmit path. Here, in contrast to the previously explained single input PA models, $f(.)$ is a nonlinear mathematical function that describes the effects of amplification as well as the effects of PA output load variation (Γ_i). (3.4) is referred to as a dual input PA model.

Until now several dual input PA models have been introduced [28–38]. Zakka in [38] proposed a memoryless dual input PA model based on Poly-Harmonic Distortion (PHD) [37] modeling approach to use in a macro transmitter modeling. Fager, et al. [35] proposed a memory polynomial dual-input model which is suitable for wideband signals. A load-dependent model is proposed by Dhar, et al. [36] which accounts for PA behavior under output load variation in MIMO arrays. In [31, 34] a dynamic dual-input PA model is developed which characterizes PA under mismatch at the input and output. These PA models are not presented for the MIMO application, but it can be applied in this context.

As an example, the structure of the memory polynomial dual-input model proposed by [35] is presented here. This model is developed based on a

third-order PHD model which includes memory effects.

$$
\begin{aligned}
b_2(n) = & \sum_{m_1=0}^{M} \underbrace{\sum_{p_1=1}^{P_1} c_{m_1,p_1} |a_1(n-m_1)|^{2p_1-1}}_{S_{21}(|a_1|)} a_1(n-m_1) + \\
& \sum_{m_2=0}^{M_2} \underbrace{\sum_{m_1=0}^{M_1} \sum_{p_2=1}^{P_2} d_{m_1,m_2,p_2} |a_1(n-m_1)|^{2(p_2-1)}}_{S_{22}(|a_1|)} a_2(n-m_2) + \\
& \sum_{m_2=0}^{M_2} \underbrace{\sum_{m_1=0}^{M_1} \sum_{p_2=2}^{P_2} e_{m_1,m_2,p_2} a_1^2(n-m_1) |a_1(n-m_1)|^{2(p_2-2)}}_{T_{22}(a_1)} a_2^*(n-m_2),
\end{aligned}
\tag{3.5}
$$

where (P_1, P_2) and (M_1, M_2) are the nonlinear model orders and memory depth, respectively.

Similar to classical S-parameters definition, the term $S_{21}(|a_1|)$ maps the incident wave a_1 to the wave b_2. Likewise, $S_{22}(|a_1|)$ maps a_2 to b_2 wave. S_{21} and S_{22} depends on the amplitude of the input wave. $T_{22}(a_1)$ is a term that depends on amplitude and phase of input wave and map conjugate of a_2 wave to b_2. The two last parts of (3.5) describe PA nonlinear behavior due to the effect of waves coming from other branches and $S_{21}(|a_1|)$ is showing the large signal gain of the PA.

3.3.1 Using interpolation functions

So far, the presented models rely on specific mathematical representations which are developed based on the knowledge about the PA behavior. In many practical applications, the PA nonlinear characteristics are achieved experimentally. Therefore, an adequate mathematical function may not be easily found. The model, which is also useful for computer simulation, can simply be a tabular representation of experimental data [19, 39, 40].

The other similar approach is to map the input-output data relationships through an interpolation function. In this way, the data points in-between the given measured ones can be estimated as well. Nowadays, computational software provides a variety of built-in interpolation functions such as piecewise linear. Therefore, with adequate experimental data points, an interpolation function can approximate the PA behavior without the constraint of a polynomial model, as described above. Piecewise interpolation function, as an example, have the advantage to be equally accurate for all points within the measured data range. Therefore, it can characterize PA

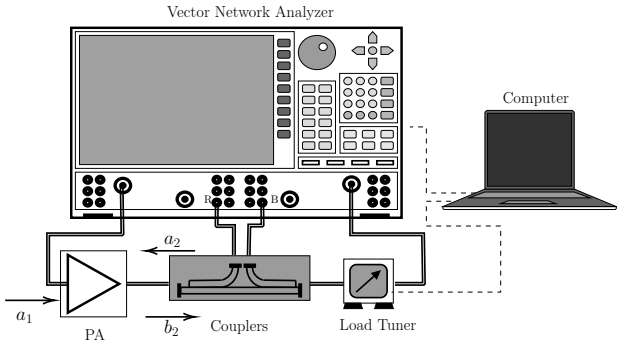

Figure 3.3: Block diagram of a conventional load-pull measurement setup.

behavior for large mismatches with reasonable accuracy. In Paper [A], we used a piecewise linear interpolation function to characterize the PA static nonlinear behavior versus different output loading conditions.

Including memory effect in the interpolation model is not trivial. One approach can be to develop an interpolation function that relates the instantaneous complex gain of PA to the instantaneous inputs and M preceding samples (memory depth).

3.4 Model Identification

Once the model structure is specified, a set of measured or simulated data representing the PA output versus known inputs is required to identify the model. The measured data is used to obtain the model coefficients or to develop an interpolation function. For single-input models, data collection for model identification is relatively straight forward. However, for dual-input models, load-pull is required to emulate a_2 waves.

3.4.1 Load-Pull Measurements

In conventional load-pull experiments, a passive tuner changes the output load impedance of the PA. The reflected wave back to the PA output, a_2, can be collected using directional couplers. Active load-pull instead uses an adjusted signal to be injected to the PA output [41, 42]. By measuring the incident and reflected waves at the PA ports, the model coefficients or interpolation function can be specified.

In Paper [A], we performed a passive load-pull measurement to develop the static interpolation function of the PA which is integrated into a beamforming Integrated Circuit (IC). Fig. 3.3 shows the block diagram of the load-pull measurement setup that was used. The input wave, a_1, is in this case a single tone continuous wave (CW) signal at 29 GHz frequency.

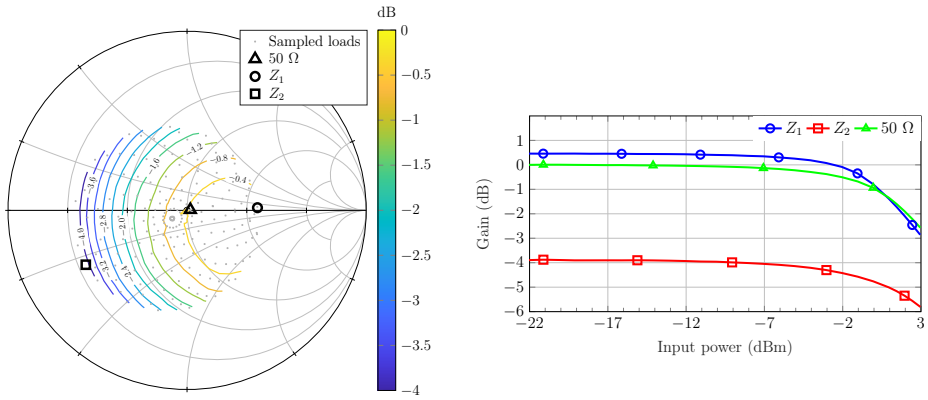

(a) (b)

Figure 3.4: a) Normalized delivered output power contours from load-pull measurement at 29 GHz. Markers are $Z_1 = 115 + j4$, $Z_2 = 11 - j12$ and 50Ω. Gray points indicate loads used during load-pull characterization, b) Normalized AM/AM for the different marked loads Z_1, Z_2 and 50 Ω. The results are normalized to the small signal measurements with a 50 Ω load.

For each level of input power and specified tuner load, a_2 and b_2 waves at the DUT interface are measured. Therefore, the AM/AM and AM/PM characteristics of the PA have been measured for all specified tuner loads.

Fig. 3.4(a) shows the normalized delivered output power contours that are obtained from the interpolated load-pull measurement data. Fig. 3.4(b) presents AM/AM plots for three different tuner loads, i.e. $Z_1 = 115 + j4$, $Z_2 = 11 - j12$ and 50 Ω. Plots are normalized to the gain values in the linear working region for the 50 Ω loading. As one can see, both the behavior and absolute levels of the AM/AM plots change with varying the loading. Similar behavior is observed for AM/PM curves. More details about the measurement scenario can be found in Paper [A].

3.4.2 Least Square Estimator

Once the measured data are collected, the least-square estimator finds the coefficients of the models which are linear in coefficients e.g. (3.2), (3.3) and (3.5) [43]. Generally, a PA model which is linear in coefficient is described as a summation of weighted (model coefficients) basis functions. For N number of PA input and output measured samples, the model can be written as

$$\mathbf{b} = \mathbf{H}(\mathbf{a})\boldsymbol{c}, \tag{3.6}$$

where $\mathbf{b}$ is a column vector containing the N measured samples of the PA output i.e. $\mathbf{b} = [b(1)..., b(N-1), b(N)]^T$. $\boldsymbol{c}$ is a column vector of the model

coefficients. $\mathbf{H}(\mathbf{a})$ is a matrix containing the evaluated nonlinear model basis functions based on known input samples, i.e. $a(n)$[1].

The least-square estimate of the model parameters can be identified as

$$\hat{\boldsymbol{c}} = (\mathbf{H}^T\mathbf{H})^{-1}\mathbf{H}^T\mathbf{b}. \tag{3.7}$$

As described earlier, in Paper [A] we applied the measured data directly to develop the interpolation function. However, it is possible to map the measured data to a memoryless dual input polynomial model using the least square technique [35].

3.5 Summary

In this chapter, an overview of PA behavioral modeling is given. First, the basic characteristics of a PA are described to the reader. Single input and dual input models were then presented for application in the transmitter model. The use of an interpolation function for modeling is introduced as an alternative to the typical polynomial based models. Finally, the model identification method and measurements are discussed. PAs are one major source of nonlinear distortion in the transmitter. In MIMO system transmitters, PAs are subject to wave coming from other branches. Therefore, developing new PA behavioral models suitable for transmitters in MIMO systems is of major interest. The use of a proper PA model is crucial for correct analysis of the active transmitter antenna array.

[1]For the dual input models, a set of $a_1(n)$ and $a_2(n)$ are used to evaluate the model basis functions.

Chapter 4

Active Antenna Transmitter Modeling

In this chapter, the analysis and modeling of active transmitter antenna arrays is explained. As it is introduced in Chapter 1, the digital and hybrid beamforming architectures are typical hardware configurations for the transmitter in MIMO systems. Both architectures are equipped with an active antenna array where each antenna element is excited with an individual PA. It is, therefore, crucial to develop an efficient methodology for the analysis of transmitters including several PAs and antennas interacting with each other.

In this chapter, first, the importance of modeling for analysis of active transmitter antenna performance is described. Then, possible modeling approaches are introduced based on the different PA and antenna array models described in Chapters 2 and 3. The description of different modeling terminologies clarifies the contribution of this thesis in relation to other published works. Our proposed modeling approach for hybrid beamforming transmitters is described in the last section. The experimental results of a 29 GHz active sub-array antenna and succeeding simulation study of a large-scale hybrid beamforming transmitter are provided in the same section. The chapter finishes with a summary.

4.1 Importance of Transmitter Modeling

The active transmitter antenna array consists of radiating antenna elements and PAs. Each of them designed and simulated individually using EM and circuit CAD tools such as Ansys HFSS, Keysight ADS, Cadence etc. Antenna EM and active circuit CAD tools are developed for full-wave and circuit-level simulation. However, when it comes to performing analysis

on the transmitter-level, such a detailed simulation (in a co-simulation or combined EM/circuit form) is neither feasible nor logical for large active antenna arrays. Furthermore, using these tools limit the investigation to the specific CAD capability and simulation results. For instance, EM and circuit CAD tools cannot deal with modulated signals in an efficient way. In [44–47] specific CAD-based approaches for the analysis of active antenna arrays are proposed. However, the proposed methods are not applicable to modulated signal analysis and transmitters serving large antenna arrays.

An efficient way to analyze an active transmitter antenna array is instead to develop an analysis framework based on antenna array and PA behavioral models. The PA and antenna array models are built from the measurement or CAD-based simulation results. The individual models can be incorporated into an active antenna analysis framework to model the transmitter behavior, see Fig. 1.3. The purpose and application of the transmitter modeling specifies the complexity of the antenna array and PA models representing their behaviors.

The modeling of a transmitter helps to find a suitable description and understanding of its behavior. The model can then be used to predict the output of the transmitter for any specific input signal or to understand observed measured results. Moreover, modeling is essential before implementing the hardware. Having adequate knowledge about the transmitter performance under realistic conditions helps to modify transmitter configuration and building blocks if possible. The other advantage is that unwanted transmitter output, such as nonlinear distortion can be predicted, and a proper compensation approach can be developed correspondingly. Furthermore, with an accurate model different signal processing algorithms can be evaluated which helps to avoid expensive and complicated measurement setups and thus improves development speed.

4.2 Modeling Techniques

The first modeling approach in this section considers a transmitter with isolated RF paths. In this active transmitter, antenna elements are weakly coupled and mutual coupling can be ignored. The second model is proposed for the transmitter with coupled RF paths, i.e. the mutual coupling between antenna elements cannot be ignored and must be considered in the transmitter analysis approach.

The terminology of this section is developed assuming that all PA and antennas are working at the same center frequency. The digital precoding/beamforming and linearization are performed in the digital signal processing unit, see Fig. 1.3. Precoding/beamforming weights are calculated

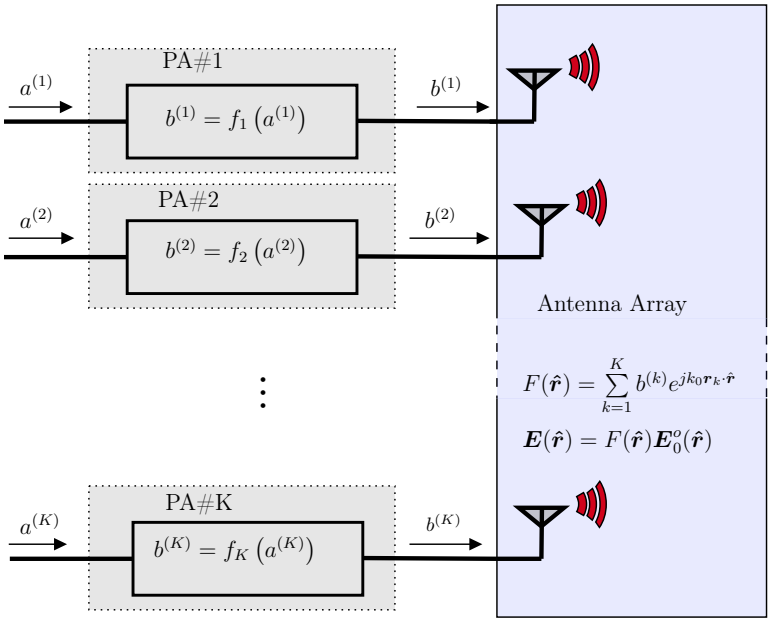

Figure 4.1: The modeling framework of active transmitter antenna array with isolated RF transmit paths

based on the channel state information and by applying proper precoding techniques such as zero-forcing or maximum ratio combining [48, 49]. The modeling formulation maps the signal incident to the PA (the baseband complex envelop of incident power wave) to the radiated field signal, i.e. the transmitter output. Here our focus is on evaluating radiated signal characteristics. The radiated far-field signal provides valuable knowledge about transmitter performance in all spatial directions as well as the user directions.

4.2.1 Isolated RF paths

Fig. 4.1 shows the analysis framework of an active transmitter antenna array with isolated branches. In this transmitter, the mutual coupling in the antenna array and in general between the branches is negligible. Therefore, as described in Sec. 3.2, a single input PA model is suitable for such a system. For a transmitter with K branches the output of each PA is

$$b_2^{(k)}(n) = f_k(a_1^{(k)}(n)), \tag{4.1}$$

where $a_1^{(k)}(n)$ is the incident signal to the PA and $b_2^{(k)}$ is the PA output in the k-th transmit path. $f_k(.)$ is the k-th PA behavorial model. A suitable antenna array model for this transmitter is introduced in Sec. 2.1. The array radiation pattern is calculated as (2.3). It is assumed that the antenna

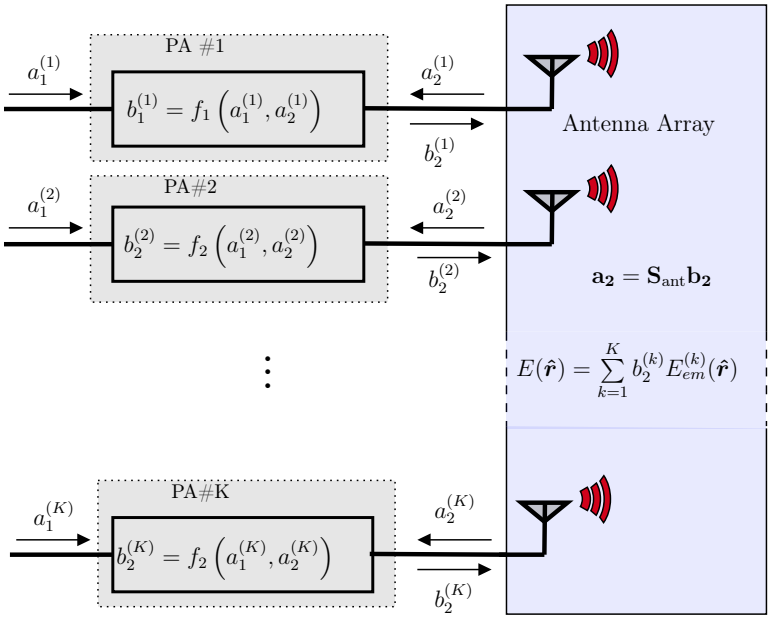

Figure 4.2: The modeling framework for active transmitter antenna array with non-negligible antenna array mutual coupling.

elements and PAs are well matched to a 50 Ω interface. Therefore, the total antenna array radiated field at the spatial direction $\hat{\boldsymbol{r}}$ and time instant n can be calculated as

$$\boldsymbol{E}(\hat{\boldsymbol{r}}, n) = \boldsymbol{E}_0^o(\hat{\boldsymbol{r}}) \sum_{k=1}^{K} b_2^{(k)}(n) e^{jk\boldsymbol{r}_k \cdot \hat{\boldsymbol{r}}}, \tag{4.2}$$

where $b_2^{(k)}(n)$ are the PA outputs which are antenna array excitations. Therefore, using (4.2) the transmitter radiated field is

$$\boldsymbol{E}(\hat{\boldsymbol{r}}, n) = \boldsymbol{E}_0^o(\hat{\boldsymbol{r}}) \sum_{k=1}^{K} f_k(a_1^{(k)}(n)) e^{jk\boldsymbol{r}_k \cdot \hat{\boldsymbol{r}}}. \tag{4.3}$$

For a weakly coupled antenna array, the elements radiation pattern, i.e. $\boldsymbol{E}_0^o(\hat{\boldsymbol{r}})$, are considered to be similar and equal to the isolated antenna element pattern. The other terms in this equation have been introduced in Sec. 2.1.

4.2.2 Coupled RF paths

Fig. 4.2 shows the analysis framework for the active transmitter antenna array with coupled antenna elements. The mutual coupling affects antenna element radiation patterns and PA outputs. The suitable PA model for this

transmitter is the dual-input model introduced in Sec. 3.3. In k-th transmit path, the output of each PA is

$$b_2^{(k)}(n) = f_k(a_1^{(k)}(n), a_2^{(k)}(n)), \tag{4.4}$$

where $f_k(.)$ is k-th PA dual input behavioral model. $a_1^{(k)}(n)$ and $b_2^{(k)}(n)$ are the PA input and output signals. $a_2^{(k)}(n)$ is the incident signal to PA output due to antenna array mismatch and mutual coupling which is determined using the antenna array S-parameters, $\mathbf{S}_{\text{ant}}$, i.e.

$$\mathbf{a_2} = \mathbf{S}_{\text{ant}}\mathbf{b_2}, \tag{4.5}$$

where $\mathbf{a_2} = [a_2^{(1)}(n), a_2^{(2)}(n), ..., a_2^{(K)}(n)]^T$ and $\mathbf{b_2} = [b_2^{(1)}(n), b_2^{(2)}(n), ..., b_2^{(K)}(n)]^T$. This model structure is suitable for antenna S-parameters that are flat over the signal bandwidth. For frequency-dependent antenna behavior, finite impulse response (FIR) filters representing antenna mismatch and coupling can be used, as in [50]. It is important to jointly solve (4.5) and (4.4) to find correct values for $b_2^{(k)}$. As described in Sec. 2.3, each antenna element radiated field is affected by mutual coupling. Therefore, the isolated element radiation pattern is not applicable and the embedded element pattern must be used. When the correct values of $b_2^{(k)}$ are found, the total radiation field is calculated as

$$\boldsymbol{E}(\hat{\boldsymbol{r}}, n) = \sum_{k=1}^{K} b_2^{(k)}(n)\boldsymbol{E}_k^{em}(\hat{\boldsymbol{r}}), \tag{4.6}$$

where $\boldsymbol{E}_k^{em}(\hat{\boldsymbol{r}})$ is the embedded element pattern of the antenna connected to the k-th PA. In an active transmitter antenna with coupled antenna elements, it is not trivial to find incident signals to the antenna elements. In k-th branch, $b_2^{(k)}$ depends on both the mismatch and the mutual coupling in the antenna array side as well as PA input signal. Two incident waves into the PA, $a_1^{(k)}$ and $a_2^{(k)}$, determine the output signal of the PA, $b_2^{(k)}$, which is also the incident wave to the k-antenna element. Implementing the interactions between the antenna array and PAs is critical for correct analysis of the active transmitter antenna array performance.

Fager, Barradas and Zakka, et al. [38, 50–52] proposed techniques where the interaction between PA and antenna array are solved to find the value of the signal at the PA and antenna interface, i.e. $b_2^{(k)}$.

Barradas et al. [52] implemented the PA and antenna S-parameter models in a MATLAB Simulink scheme such that the signal returning from a antenna array element, i.e. $a_2^{(k)}$, is fed back to the dual input PA model. In this way, a joint analysis scheme is provided for the transmitter performance.

In [38], the antenna active impedance is considered as PA output load. PA outputs, $b_2^{(k)}$, are determined using a dual input PHD models. Fager, et al. [50, 51] developed a transmitter model which is formulated as $\mathbf{b} = f(\mathbf{a}, \mathbf{S}_{\text{ant}})$. In this work, proposing a closed-form analytical solution is possible since the applied PA model is linear with regards to the $\mathbf{a_2}$ waves. Providing an analytical solution is not straightforward for the transmitter with more complex PA models.

4.3 Proposed Modeling Technique

The complexity and cost of digital beamforming architectures at mmWave frequency bands, promotes the use of hybrid beamforming MIMO systems. Therefore, in Paper [A], we developed a hardware-oriented model for hybrid beamforming transmitters. In this section, the proposed modeling technique is described. The proposed model can be used in both digital and hybrid beamforming architectures. However, the notation is developed for the hybrid beamforming transmitter case.

4.3.1 Model Algorithm

Fig. 1.2 shows the block diagram of a typical hybrid beamforming transmitter. In this configuration, beamforming is divided in digital and analog beamforming domains. The hybrid beamforming transmitter has K RF transmit paths, each of them connected to an L-channel beamforming IC. Amplification and phase shifting is performed to the output channels via analog beamforming ICs. In total, there are LK RF output channels connected to the large-scale antenna array. Fig. 4.3 shows the analysis framework for the hybrid beamforming transmitter. It is assumed that antenna array mutual coupling cannot be ignored. Here, instead of a PA, the model for the k-th channel of beamforming IC is described as

$$b_2^{(k,l)} = f_{(k,l)}(a_1^{(k)}, a_2^{(k,l)})e^{j\phi_{(k,l)}}, \quad \text{with} \quad l = 1:L, k = 1:K, \tag{4.7}$$

where the signal $a_1^{(k)}$ is the common input to the channels of the k-th beamforming IC. $a_2^{(k,l)}$ is the incident wave to the output of l-th channel of the k-th beamforming IC. $\phi_{(k,l)}$ is the analog beamforming phase shifts. $f_{(k,l)}(.)$ is the interpolation dual input model of l-th channel of k-th beamforming IC. The interpolation models are introduced in Sec. 3.3.1. The antenna array model is similar to the one used in Sec. 4.2.2. Therefore (4.5), S-parameters, represents antenna array mismatch and mutual coupling and (2.9) stands for antenna array radiated field. In Paper [A] we propose an iterative algorithm

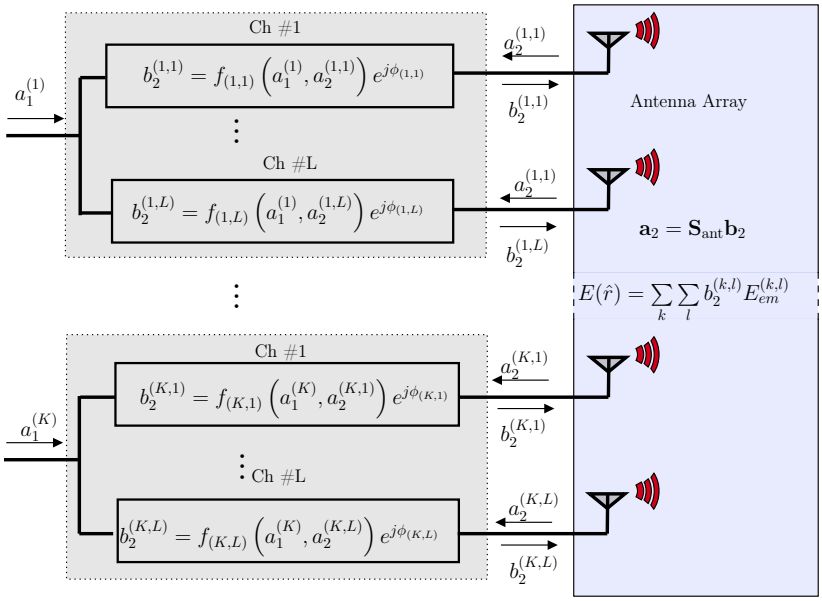

Figure 4.3: The modeling framework for a hybrid beamforming transmitter.

to find $b_2^{(k,l)}$, see Algorithm 4.1. The iterative algorithm starts with the assumption of no reflection and no mismatch at the beamforming IC outputs, i.e. $a_2^{(k,l)} = 0$. In each iteration, (4.7) and (4.5) are evaluated. After a few iterations, N_{itr}, the algorithm converges to a steady value for $a_2^{(k,l)}$.

Once $b_2^{(k,l)}$ are found, the total radiated field is calculated as

$$\boldsymbol{E}(\hat{\boldsymbol{r}}) = \sum_{k=1}^{K} \sum_{l=1}^{L} b_2^{(k,l)} \boldsymbol{E}_{em}^{(k,l)}(\hat{\boldsymbol{r}}), \tag{4.8}$$

where $\boldsymbol{E}_{em}^{(k,l)}$ are embedded element patterns of the antenna elements. For evaluating hybrid beamforming transmitter performance with modulated signal inputs, the algorithm is executed per time step n.

About Active Impedance

The changes in the impedance seen by each PA, which is the antenna active impedance, impact its output and consequently the antenna array radiated signal. In Sec. 2.3.2 the active impedance is introduced assuming ideal array excitation. The actual antenna active reflection coefficient, which takes into account the impacts of the antenna array and PAs interactions, is calculated as

$$\Gamma_{\text{actual}}^{(k,l)} = \frac{a_2^{(k,l)}}{b_2^{(k,l)}(a_1^{(k)}, a_2^{(k,l)})}, \tag{4.9}$$

Algorithm 4.1 Iterative algorithm to obtain beamforming IC output

Input:

$a_1^{(k)}$	Input signals
$f_{(k,l)}$	Beamforming IC channels interpolation model
$\mathbf{S}_{\text{ant}}$	Antenna array S-parameters
$\phi_{(k,l)}$	Analog phase shifts
$a_{2,0}^{(k,l)} = 0$	Algorithm initialization ($i = 0$)

for i=1 to N_{itr} **do**
  for all k **do**
    for all l **do**
      $b_{2,i}^{(k,l)} = f_{(k,l)}(a_1^{(k)}, a_{2,i}^{(k,l)})e^{j\phi_{(k,l)}}$
    end for
  end for
  $\mathbf{b_2} = [b_{2,i}^{(1,1)}, ..., b_{2,i}^{(1,L)}, b_{2,i}^{(2,1)}, ..., b_{2,i}^{(K,L)}]^T$
  $\mathbf{a_2} = \mathbf{S}_{\text{ant}}\mathbf{b_2}$
  with
  $\mathbf{a_2} = [a_{2,i+1}^{(1,1)}, ..., a_{2,i+1}^{(1,L)}, a_{2,i+1}^{(2,1)}, ..., a_{2,i+1}^{(K,L)}]^T$
  $i = i + 1$,
end for
Output:

$b_2^{(k,l)}$	Output signals for all n, $l = 1 : L$ and $k = 1 : K$.

where $b_2^{(k,l)}$ are achieved from Algorithm 4.1. In Paper [A], the active reflection coefficient obtained from (4.9) of the evaluated hybrid beamforming subarray module shows considerable difference relative to the traditional case, where PA load dependence is neglected.

4.4 Evaluating a 29 GHz Hybrid Beamforming Subarray Module

The accuracy of the proposed method explained in Sec. 4.3 was evaluated using measurements of a 29 GHz hybrid beamforming transmitter subarray module. To assess the subarray module performance, first the beamforming IC and the subarray antenna were characterized. Then the proposed iterative algorithm predicts the subarray module performance for various beam steering scenarios. As introduced in Sec. 2.2, the beam steering means applying proper phase-shifts to antenna element in a way the antenna beam is steered to different directions. Next, over-the-air (OTA) measurements were performed to validate the predicted results in terms of the radiation

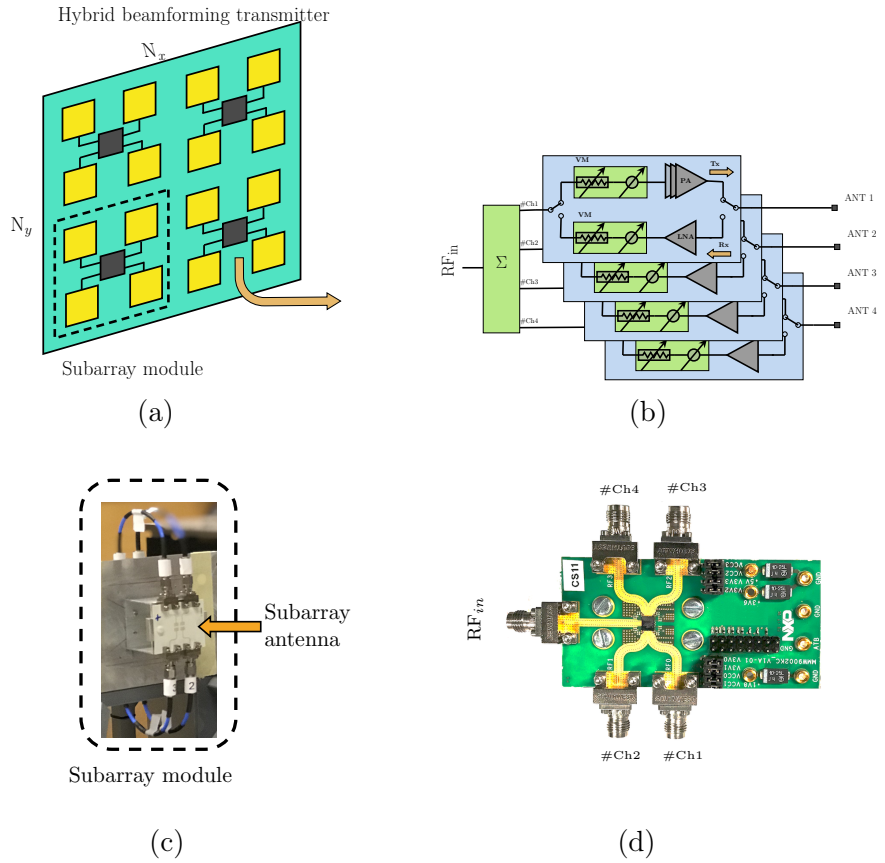

Figure 4.4: Hybrid beamforming transmitter and its building blocks. a) Subarray module, b) Beamforming IC block diagram, c) Picture of implemented subarray module, d) Evaluation board of the quad channel beamforming IC.

pattern and far-field nonlinear distortion.

The validation measurement in Paper [A] was performed for the beam steering scenario. However, modeling can be applied to a hybrid digital and analog beamforming scenario when proper digital and analog weights are applied to the transmit signals.

4.4.1 Hardware Configuration

Fig. 4.4 (a) shows the hardware configuration of a typical hybrid beamforming transmitter and its building blocks. The transmitter's building blocks are 2×2 subarray antennas, which are driven by individual beamforming ICs.

A beamforming IC is a multi-channel component that includes Tx/Rx blocks integrated into an RF frontend. The TX/RX blocks include phase shifters, T/R switches, attenuators, PAs, and low noise amplifiers, see Fig. 4.4

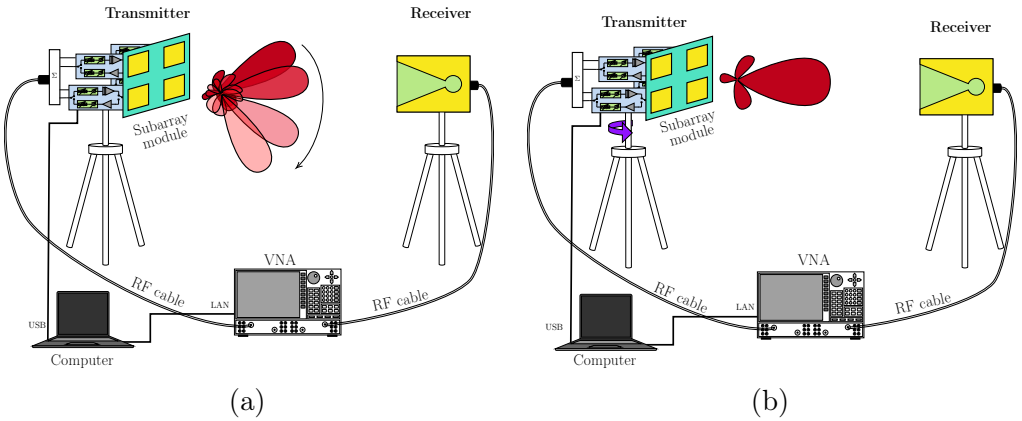

Figure 4.5: Block diagram of the setup for a) far-field signal distortion measurement, b) radiation pattern measurement.

(b). A typical hybrid beamforming transmitter employs beamforming ICs for applying independent analog beamforming weights to each of the output channels.

In Paper [A], the test case is a subarray module consist of 2×2 planar microstrip patch antenna array which is connected to an evaluation board of a quad-channel beamforming IC from NXP semiconductors. The beamforming IC operates at 26.5-29.5 GHz. In the transmit mode, it consists of one input and four RF output channels. The 2×2 subarray antenna includes rectangular microstrip patch elements working at 29 GHz frequency. Fig. 4.4 (c) and (d) show the picture of the tested subarray module and the beamforming IC evaluation board.

4.4.2 Experimental Setup and Scenarios

The beamforming IC and antenna subarray must be characterized to evaluate the subarray module performance. As described in Sec. 3.4.1, the beamforming IC model was identified using passive load-pull measurements performed at 29 GHz. The static behavioral model of the beamforming IC channels was obtained using a MATLAB linear interpolation function. The measured antenna array S-parameters and EM simulated embedded element patterns were used in the modeling framework shown in Fig. 4.3. The highest measured coupling happened between side by side elements, and was around -12 dB. The antenna array and load-pull characterization procedure are described in details in Paper [A].

Over The Air (OTA) measurements, were performed to validate the proposed transmitter modeling approach. Fig. 4.5 shows the block diagram of the OTA measurement setup. It includes the 2×2 subarray module

as the transmitter, a single antenna as the receiver and a VNA for signal generation and reception. The input to the subarray module is a single tone signal at 29 GHz generated by the VNA.

In one measurement scenario, the distortion of the radiated signal was evaluated versus different steer angles. Fig. 4.5(a) shows the the OTA block diagram for assessing far-field nonlinear distortion. The subarray module, as the transmitter, is set to steer the beam to $|Az_{\mathrm{s}}| < 80°$, $|El_{\mathrm{s}}| < 75°$. The input power swept from -22 to 3 dBm to push the PAs of the beamforming IC a few dB into compression. The OTA measurements of AM/AM and AM/PM are used to characterize the radiated signal distortion in the far-field.

In another scenario, the transmitter was set to steer the beam toward three specific steer angles. For each steer angle, the radiation pattern in the x-z plane was measured. In this scenario, the transmitter antenna was rotated along its vertical axis, The relative values of the received power versus rotation angle is the radiation pattern. Fig. 4.5(b) illustrates the block diagram of radiation pattern measurement scenarios. Both measurement scenarios can be used to effectively validate the proposed transmitter modeling.

4.4.3 Experimental results

The experimental results related to the scenarios explained in Sec. 4.4.2 are presented here. Results include radiation pattern and AM/AM and AM/PM distortions in the far-field.

Far-Field Signal Distortion

The OTA measured AM/AM and AM/PM distortion results correspond to the amplitude and phase of the received signal versus input power to subarray module, see Fig. 4.5(a). The amplitude and phase variation of calculated far-field radiation pattern represents the modeled AM/AM and AM/PM distortion. The difference between small signal and peak power gain and phase is denoted as *amplitude and phase compression* to quantify the AM/AM and AM/PM distortion behavior with two single values.

Fig. 4.6 shows the normalized received power together with amplitude and phase compression variation in the far-field for different azimuth and elevation steering angles, $|Az_{\mathrm{s}}| < 80°$, $|El_{\mathrm{s}}| < 75°$. The measured results shows that nonlinear distortion depends significantly on steering angle. The RMS error of amplitude and phase compression values is about 0.18 dB and 1.6 degrees respectively. In general, the difference between the predicted and measured results is acceptable considering uncertainties in the measurement setup. In Paper [A] more details about the validation results are presented.

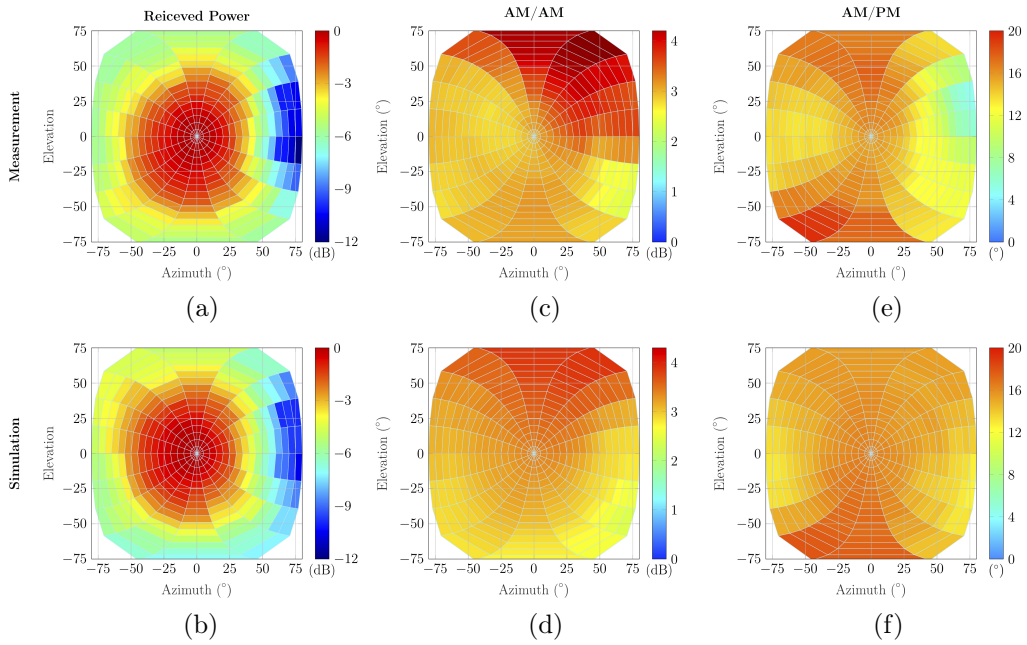

Figure 4.6: Normalized received power together with amplitude and phase compression variation in the far-field for different azimuth and elevation steering angles, $|Az_{\mathrm{s}}| < 80°$, $|El_{\mathrm{s}}| < 75°$. Normalized received power: a) OTA experiment b) Simulation. Amplitude compression: c) OTA experiment d) Simulation. Phase compression: e) OTA experiment f) Simulation. The RMS error between simulation and measurement of the amplitude and phase compression is 0.18 dB and 1.6 degrees, respectively.

Far-Field Radiation Pattern

Fig. 4.7 shows the measured and simulated radiation pattern for steered angles $El_s = 0°, Az_s = -30°, 0°$. The input power is 0 dBm and with this power, the PAs are in compression. Prediction results were obtained from (4.8) using simulation based embedded element patterns. The nonlinearity effects on the radiation pattern were not significant for this subarray antenna. In [46], an unwanted sidelobe appears due to PA nonlinear effect on the antenna array performance. The nonlinear PA and antenna interactions have a significant influence on the signal distortion as is shown in Fig. 4.6. The presented method is effectively validated with a single tone CW measurement. However, it can also be used to investigate the dynamic nonlinear behavior of the modulated signal if the signal bandwidth is relatively low. A requirement is then that the antenna array and beamforming IC should have relatively constant characteristics within the signal bandwidth, as explained in Sec. 3.1.1.

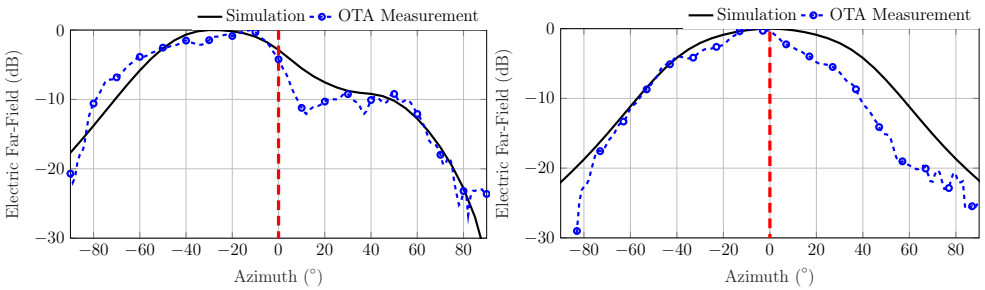

(a) (b)

Figure 4.7: H-plane radiation pattern ($El = 0°$) versus steered angle: a) $(Az_s, El_s) = (-30°, 0°)$, b) $(Az_s, El_s) = (0°, 0°)$, The red dashed line shows the boresight angle.

4.5 Transmitter Linearity Study

Linearity is a crucial requirement for any wireless transmitter. Therefore, linearization algorithms, with a focus on DPD, are part of most MIMO system transmitters. A variety of DPD techniques have been proposed to compensate transmitter nonlinearity in MIMO systems [53–59]. For hybrid beamforming transmitters, beam-dependent DPD schemes have shown to be an efficient solution [53,55,56]. Therefore, it is important to assess transmitter performance in conjunction with DPD through a reliable transmitter model. This helps in the process of developing DPD techniques as well as designing suitable active antenna arrays for transmitters employing DPDs.

In this section, different large-scale hybrid beamforming transmitters are evaluated from a linearity perspective through a simulation study. The linearity is being evaluated for a beam steering scenario using the proposed algorithm in Sec. 4.3. Therefore, all subarrays are assumed to have a common input signal. An ideal beam-dependent predistorter is designed based on the predicted far-field static nonlinear distortion. The behavior of the linearized transmitter is evaluated for all steered beams. The inputs to the transmitter model algorithm, such as the antenna array S-parameters and embedded element patterns, are extracted from EM simulations. The beamforming IC is the one that was characterized in Sec. 3.4.1. The focus of this section is not on developing a linearization or DPD technique. This study is performed to demonstrate the potential of our proposed method for the linearity analysis of large-scale hybrid beamforming transmitter systems where beam-dependent DPD is applied.

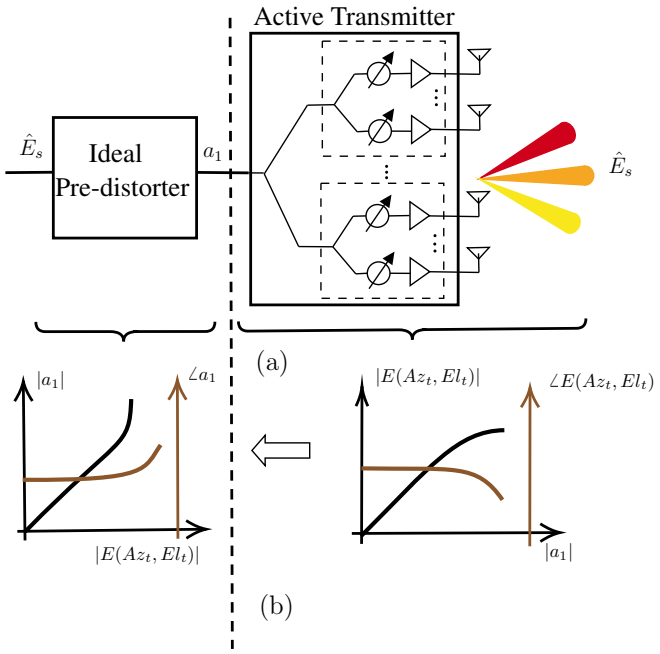

Figure 4.8: a) Structure of hybrid beamforming transmitter utilizing an ideal predistorter. b) The conceptual representation of the transmitter transfer AM/AM and AM/PM function and corresponding pre-distorter.

4.5.1 Ideal predistorter

Fig. 4.8 illustrates the conceptual representation for developing the pre-distorter AM/AM and AM/PM functions. The considered ideal predistorter is designed to linearize the transmitter for one specific beam direction, i.e. (Az_t, El_t). First, the transmitter radiated far-field is evaluated for the target steered beam (Az_t, El_t). $E(Az_t, El_t, |a_1|)$ is obtained by applying the method described in Sec. 4.3. The power of the input signal is swept until the transmitter is a few dB in compression. The ideal pre-distorter function is obtained by swapping input and output of the $E(Az_t, El_t, |a_1|)$ function. $|E(Az_t, El_t, |a_1|)|$ as the input, and $|a_1|$ as the output are interpolated to obtain the predistorter AM/AM function. The AM/PM pre-distorter function is the minus of $\angle E(Az_t, El_t, |a_1|)$.

4.5.2 Simulation results

Hybrid beamforming transmitters with two antenna array configurations $(N_x \times N_y)$, 8×8 and 16×4, are designed in CST and studied here, see Fig. 2.2 for the antenna configuration. The coupling level is -12 dB and -20 dB between elements in x and y direction, respectively. Each 2×2 subarray antenna are driven by individual beamforming ICs. The beamforming IC is

the one characterized in Sec. 3.4.1.

The behavior of the beamforming transmitter combined with the ideal pre-distorter is evaluated for all beam steering cases. $\hat{E}_s(n)$ is the desired far-field signal at the time instance n. $E_s(n)$ is the farfield signal at the main beam of each individual steered beam. A single carrier LTE communication signal with an 8.5 dB Peak-to-Average Power Ratio (PAPR) and 20 MHz bandwidth is selected as $\hat{E}_s(n)$. The normalized mean square error (NMSE) is considered as the figure of merit for evaluating the linearity of each steering beam. The NMSE is calculated by:

$$\text{NMSE} = \frac{\sum_{n=1}^{N} |\alpha E_{\text{s}}(n) - \hat{E}_{\text{s}}(n)|^2}{\sum_{n=1}^{N} |\alpha E_{\text{s}}(n)|^2}, \tag{4.10}$$

where N is the total number of time samples. α is a complex scaling factor which is calculated for each steered beam to eliminate the effects of gain and output power variations in different steering directions.

The 16×4 transmitter is linearized for the steer angles $(Az_t, El_t) = (0, 0)^\circ, (50, 0)^\circ, (30, 25)^\circ$, and the 8×8 transmitter is linearized for $(Az_t, El_t) = (0, 0)^\circ$. Fig. 4.9 shows the linearity (NMSE) of the linearized transmitters for steered beam $|Az_s| < 80^\circ, |El_s| < 75^\circ$. In each configuration, in the direction (Az_t, El_t) the transmitter with ideal predistorter is ideally linear. It can be seen that the array configuration and coupling level between elements in x or y direction affects the linearity variation. In this study, the nonlinear distortion is very low for all cases and steered beams. However, the NMSE variation between different beams is significant. The other observation is that linearity has a diagonal symmetry behavior. This happens because beams at (Az_s, El_s) and $(-Az_s, -El_s)$ are identical for an equally spaced ideal rectangular array.

Generally, the linearity behavior relies on the specific beam direction which is aimed to be fully linearized [53, 55, 56]. This is an important observation which should carefully take into account for a transmitter in the design stage.

4.6 Summary

In this chapter, the existing approaches for the modeling of active transmitter antenna arrays are introduced. The proposed modeling approach and its iterative algorithm are explained, and validation experimental results are presented. Finally, the proposed transmitter analysis method is applied to predict the linearity of large-scale transmitters when an ideal beam-dependent linearization is used.

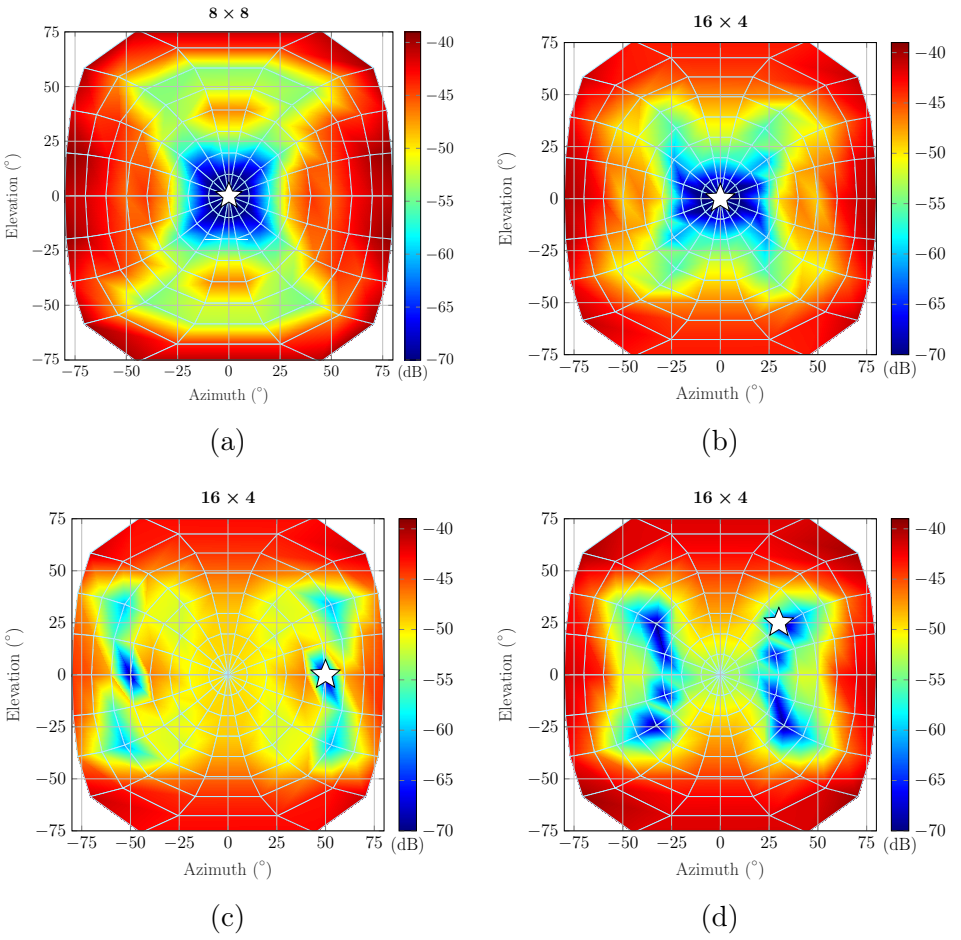

Figure 4.9: Nonlinear distortion in the far-field versus steering angle for a) 8×8 array linearized for the beam at $(Az_t, El_t) = (0, 0)°$, b) 16×4 array linearized for $(Az_t, El_t) = (0, 0)°$, c) 16×4 array linearized for $(Az_t, El_t) = (50, 0)°$, and d) 16×4 array linearized for $(Az_t, El_t) = (30, 25)°$. The results are presented in terms of normalized mean square error for an LTE signal with 8.5 peak-to-average power ratio. The white filled star represents the direction that the beam-dependent DPD is optimized for.

Chapter 5

Conclusions and Future Work

MIMO systems utilize active transmitter antenna arrays for higher energy efficiency, higher capacity and increased flexibility. The performance analysis of any transmitter is crucial before implementing it. Due to a large number of PAs and antennas, the analysis of a MIMO system transmitter is more challenging compared to traditional transmitters. In addition, isolators are too bulky and cannot typically be used in mmWave active antenna arrays. Therefore, the interaction between the antenna array and PAs becomes more critical for transmitter modeling. The coupling and mismatch in the antenna array change the PA output load and consequently the output signal. The PA outputs variation affects the total antenna array radiated signal. Therefore, a newly adapted analysis framework that includes such interactions is required for active transmitter antenna arrays analysis.

In this thesis, we have combined the nonlinear PA model with antenna array characteristics in an iterative algorithm to model the active transmitter antenna array performance. The transmitter model considers PA and antenna array interactions which are significant in mmWave MIMO transmitters. The model is based on the interpolation of load-pull measured data and is a feasible method for modeling at mm-wave frequencies.

The reliability of the proposed modeling approach has been validated using the measurement of a mmWave hybrid beamforming transmitter subarray module for a beam steering scenario. The OTA measurement results prove the validity of the model as both radiation pattern and far-field distortion are in good agreement with simulation results. The potential of the method is demonstrated with the analysis of large-scale transmitters in a realistic beam-linearized application scenario. The proposed linearity analysis is beneficial for assessing DPD techniques and evaluating the performance of transmitters employing DPDs.

5.1 Future Work

The topic of transmitter modeling still presents several possible directions for future work. A variety of investigations about PA and antenna array different characteristics on the transmitter performance can be performed. These characteristics can be antenna array configuration, mismatch, and mutual coupling level as well as PA nonlinearity and load-dependency. The transmitter performance includes nonlinear distortion, radiation pattern, and output power. For instance, the effect of regular and irregular antenna arrays can be studied on the transmitter linearity. This investigation leads to find a suitable antenna array configuration for improving transmitter linearity performance. In general, such investigations can provide design guides and criteria for developing antenna arrays and PAs.

The small physical dimension of mmWave active antenna arrays together with the utilization of low-efficiency PAs, create significant thermal issues for mmWave MIMO transmitters [60–62]. Among transmitter components, PAs are highly temperature-dependent devices which also contribute significantly to heat dissipation. Therefore, it is crucial to incorporate PA thermal behavior into the transmitter analysis framework. For this purpose, the adapted electro-thermal model of PAs can be exploited for developing a multi-physics transmitter model.

References

[1] P. Jonsson, "Ericsson mobility report," *Nov*, 2019.

[2] W. Roh *et al.*, "Millimeter-wave beamforming as an enabling technology for 5G cellular communications: Theoretical feasibility and prototype results," *IEEE Commun. Mag.*, vol. 52, no. 2, pp. 106–113, 2014.

[3] T. S. Rappaport *et al.*, "Millimeter wave mobile communications for 5G cellular: It will work!" *IEEE Access*, vol. 1, no. 1, pp. 335–349, 2013.

[4] Z. Pi and F. Khan, "An introduction to millimeter-wave mobile broadband systems," *IEEE Commun. Mag.*, vol. 49, no. 6, 2011.

[5] A. Ghosh, T. A. Thomas, M. C. Cudak, R. Ratasuk, P. Moorut, F. W. Vook, T. S. Rappaport, G. R. MacCartney, S. Sun, and S. Nie, "Millimeter-wave enhanced local area systems: A high-data-rate approach for future wireless networks," *IEEE J. Select. Areas Commun.*, vol. 32, no. 6, pp. 1152–1163, 2014.

[6] H. T. Friis, "A note on a simple transmission formula," *Proceedings of the IRE*, vol. 34, no. 5, pp. 254–256, 1946.

[7] E. G. Larsson, O. Edfors, F. Tufvesson, and T. L. Marzetta, "Massive MIMO for next generation wireless systems," *IEEE Commun. Mag.*, vol. 52, no. 2, pp. 186–195, 2014.

[8] E. Bjornson, L. Van der Perre, S. Buzzi, and E. G. Larsson, "Massive MIMO in sub-6 GHz and mmwave: Physical, practical, and use-case differences," *IEEE Wireless Communications*, vol. 26, no. 2, pp. 100–108, 2019.

[9] I. Ahmed, H. Khammari, A. Shahid, A. Musa, K. S. Kim, E. De Poorter, and I. Moerman, "A survey on hybrid beamforming techniques in 5G: Architecture and system model perspectives," *IEEE Commun. Surv. & Tut.*, vol. 20, no. 4, pp. 3060–3097, 2018.

[10] F. Sohrabi and W. Yu, "Hybrid analog and digital beamforming for mmWave OFDM large-scale antenna arrays," *IEEE J. Select. Areas Commun.*, vol. 35, no. 7, pp. 1432–1443, 2017.

[11] A. Alkhateeb, O. El Ayach, G. Leus, and R. W. Heath, "Hybrid precoding for millimeter wave cellular systems with partial channel knowledge," in *Proc. Inf. Theo. Appl. Workshop (ITA)*, pp. 1–5.

[12] P. Kildal, *Foundations of Antennas: A Unified Approach*, 2015. [Online]. Available: http://www.kildal.se/

[13] C. A. Balanis, *Antenna Theory: Analysis and Design.* Wiley-Interscience, 2005.

[14] R. J. Mailloux, *Phased array antenna handbook.* Artech House antennas and propagation library, 2005.

[15] D. M. Pozar, "The active element pattern," *IEEE Trans. Antennas Propag.*, vol. 42, no. 8, pp. 1176–1178, 1994.

[16] D. Nopchinda and K. Buisman, "Measurement technique to emulate signal coupling between power amplifiers," *IEEE Transactions on Microwave Theory and Techniques*, vol. 66, no. 4, pp. 2034–2046, 2018.

[17] F. H. Raab, P. Asbeck, S. Cripps, P. B. Kenington, Z. B. Popovic, N. Pothecary, J. F. Sevic, and N. O. Sokal, "Power amplifiers and transmitters for RF and microwave," *IEEE Transactions on Microwave Theory and Techniques*, vol. 50, no. 3, pp. 814–826, 2002.

[18] M. Isaksson, D. Wisell, and D. Ronnow, "A comparative analysis of behavioral models for RF power amplifiers," *IEEE Transactions on Microwave Theory and Techniques*, vol. 54, no. 1, pp. 348–359, 2006.

[19] F. M. Ghannouchi, O. Hammi, and M. Helaoui, *Behavioral modeling and predistortion of wideband wireless transmitters.* John Wiley & Sons, 2015.

[20] O. Hammi, S. Boumaiza, and F. M. Ghannouchi, "On the robustness of digital predistortion function synthesis and average power tracking for highly nonlinear power amplifiers," *IEEE Transactions on Microwave Theory and Techniques*, vol. 55, no. 6, pp. 1382–1389, 2007.

[21] N. Le Gallou, J. M. Nebus, E. Ngoya, and H. Buret, "Analysis of low frequency memory and influence on solid state hpa intermodulation characteristics," in *2001 IEEE MTT-S International Microwave Sympsoium Digest (Cat. No.01CH37157)*, vol. 2, 2001, pp. 979–982 vol.2.

[22] J. C. Pedro and S. A. Maas, "A comparative overview of microwave and wireless power-amplifier behavioral modeling approaches," *IEEE Transactions on Microwave Theory and Techniques*, vol. 53, no. 4, pp. 1150–1163, 2005.

[23] J. Wood, *Behavioral modeling and linearization of RF power amplifiers*. Artech House, 2014.

[24] A. Zhu and T. J. Brazil, "An overview of volterra series based behavioral modeling of RF/microwave power amplifiers," in *2006 IEEE Annual Wireless and Microwave Technology Conference*, 2006, pp. 1–5.

[25] J. Kim and K. Konstantinou, "Digital predistortion of wideband signals based on power amplifier model with memory," *Electronics Letters*, vol. 37, no. 23, pp. 1417–1418, 2001.

[26] D. R. Morgan, Z. Ma, J. Kim, M. G. Zierdt, and J. Pastalan, "A generalized memory polynomial model for digital predistortion of RF power amplifiers," *IEEE Transactions on Signal Processing*, vol. 54, no. 10, pp. 3852–3860, 2006.

[27] Lei Ding and G. T. Zhou, "Effects of even-order nonlinear terms on predistortion linearization," in *Proceedings of 2002 IEEE 10th Digital Signal Processing Workshop, 2002 and the 2nd Signal Processing Education Workshop.*, 2002, pp. 1–6.

[28] A. Abdelhafiz, L. Behjat, F. M. Ghannouchi, M. Helaoui, and O. Hammi, "A high-performance complexity reduced behavioral model and digital predistorter for MIMO systems with crosstalk," *IEEE Transactions on Communications*, vol. 64, no. 5, pp. 1996–2004, 2016.

[29] D. Saffar, N. Boulejfen, F. M. Ghannouchi, A. Gharsallah, and M. Helaoui, "Behavioral modeling of MIMO nonlinear systems with multivariable polynomials," *IEEE Transactions on Microwave Theory and Techniques*, vol. 59, no. 11, pp. 2994–3003, 2011.

[30] S. Amin, P. N. Landin, P. Händel, and D. Rönnow, "Behavioral modeling and linearization of crosstalk and memory effects in RF MIMO transmitters," *IEEE Trans. Microw. Theory Techn.*, vol. 62, no. 4, pp. 810–823, 2014.

[31] H. Zargar, A. Banai, and J. C. Pedro, "A new double input-double output complex envelope amplifier behavioral model taking into account source and load mismatch effects," *IEEE Transactions on Microwave Theory and Techniques*, vol. 63, no. 2, pp. 766–774, 2015.

[32] J. Cai, R. Gonçalves, and J. C. Pedro, "A new complex envelope behavioral model for load mismatched power amplifiers," *International Journal of RF and Microwave Computer-Aided Engineering*, vol. 27, no. 6, p. e21097, 2017.

[33] F. M. Barradas, T. R. Cunha, and J. C. Pedro, "Digital predistortion of RF PAs for MIMO transmitters based on the equivalent load," in *2017 Integrated Nonlinear Microwave and Millimetre-wave Circuits Workshop (INMMiC)*, 2017, pp. 1–4.

[34] H. Zargar, A. Banai, and J. C. Pedro, "DIDO behavioral model extraction setup using uncorrelated envelope signals," in *2015 European Microwave Conference (EuMC)*, 2015, pp. 646–649.

[35] C. Fager, K. Hausmair, K. Buisman, K. Andersson, E. Sienkiewicz, and D. Gustafsson, "Analysis of nonlinear distortion in phased array transmitters," in *Proc. Workshop Integ. Nonlinear Microw. Millim. Wave Circuits (INMMiC)*, Apr. 2017, pp. 1–4.

[36] S. K. Dhar, A. Abdelhafiz, M. Aziz, M. Helaoui, and F. M. Ghannouchi, "A reflection-aware unified modeling and linearization approach for power amplifier under mismatch and mutual coupling," *IEEE Trans. Microw. Theory Techn.*, no. 99, pp. 1–11, 2018.

[37] D. Root *et al.*, "Polyharmonic distortion modeling," *IEEE Microw. Mag.*, vol. 7, no. 3, pp. 44–57, 2006.

[38] G. Z. El Nashef, F. Torres, S. Mons, T. Reveyrand, T. Monédière, E. Ngoya, and R. Quéré, "EM/circuit mixed simulation technique for an active antenna," *IEEE Antennas Wireless Propag. Lett.*, vol. 10, pp. 354–357, 2011.

[39] F. M. Ghannouchi and O. Hammi, "Behavioral modeling and predistortion," *IEEE Microwave Magazine*, vol. 10, no. 7, pp. 52–64, 2009.

[40] O. Hammi, F. M. Ghannouchi, S. Boumaiza, and B. Vassilakis, "A data-based nested LUT model for RF power amplifiers exhibiting memory effects," *IEEE Microwave and Wireless Components Letters*, vol. 17, no. 10, pp. 712–714, 2007.

[41] Y. Takayama, "A new load-pull characterization method for microwave power transistors," in *1976 IEEE-MTT-S International Microwave Symposium*, 1976, pp. 218–220.

[42] S. Gustafsson, M. Thorsell, and C. Fager, "A novel active load-pull system with multi-band capabilities," in *81st ARFTG Microwave Measurement Conference*, 2013, pp. 1–4.

[43] S. M. Kay, *Fundamentals of statistical signal processing*. Prentice Hall PTR, 1993.

[44] V. Rizzoli, A. Costanzo, D. Masotti, M. Aldrigo, F. Donzelli, and V. Degli Esposti, "Integration of non-linear, radiation, and propagation CAD techniques for MIMO link design," *J. Int. Microw. Wireless Tech.*, vol. 4, no. 2, pp. 223–232, 2012.

[45] V. Rizzoli, A. Costanzo, P. Spadoni, F. Donzelli, D. Masotti, and E. M. Vitucci, "A CAD procedure for MIMO link estimation by the combination of nonlinear, electromagnetic and propagation analysis techniques," in *Proc. IEEE MTT-S Int. Microw. Symp. Dig.*, 2008, pp. 927–930.

[46] M. Romier, A. Barka, H. Aubert, J.-P. Martinaud, and M. Soiron, "Load-pull effect on radiation characteristics of active antennas," *IEEE Antennas Wireless Propag. Lett.*, vol. 7, pp. 550–552, 2008.

[47] H. Aliakbari, A. Abdipour, A. Costanzo, D. Masotti, R. Mirzavand, and P. Mousavi, "Far-field-based nonlinear optimization of millimeter-wave active antenna for 5G services," *IEEE Trans. Microw. Theory Techn.*, vol. 67, no. 7, pp. 2985–2997, 2019.

[48] M. Joham, W. Utschick, and J. A. Nossek, "Linear transmit processing in MIMO communications systems," *IEEE Transactions on Signal Processing*, vol. 53, no. 8, pp. 2700–2712, 2005.

[49] H. Q. Ngo, *Massive MIMO: Fundamentals and system designs*. Linköping University Electronic Press, 2015, vol. 1642.

[50] K. Hausmair, S. Gustafsson, C. Sánchez-Pérez, P. N. Landin, U. Gustavsson, T. Eriksson, and C. Fager, "Prediction of nonlinear distortion in wideband active antenna arrays," *IEEE Transactions on Microwave Theory and Techniques*, vol. 65, no. 11, pp. 4550–4563, 2017.

[51] C. Fager, X. Bland, K. Hausmair, J. Chani Cahuana, and T. Eriksson, "Prediction of smart antenna transmitter characteristics using a new behavioral modeling approach," in *2014 IEEE MTT-S International Microwave Symposium (IMS2014)*, 2014, pp. 1–4.

[52] F. M. Barradas, P. M. Tomé, J. M. Gomes, T. R. Cunha, P. M. Cabral, and J. C. Pedro, "Power, linearity, and efficiency prediction for MIMO arrays with antenna coupling," *IEEE Transactions on Microwave Theory and Techniques*, vol. 65, no. 12, pp. 5284–5297, 2017.

[53] E. Ng, Y. Beltagy, G. Scarlato, A. B. Ayed, P. Mitran, and S. Boumaiza, "Digital predistortion of millimeter-wave RF beamforming arrays using low number of steering angle-dependent coefficient sets," *IEEE Trans. Microw. Theory Techn.*, vol. 67, no. 11, pp. 4479–4492, 2019.

[54] L. Liu, W. Chen, L. Ma, and H. Sun, "Single-PA-feedback digital predistortion for beamforming MIMO transmitter," in *Proc. IEEE Int. Conf. Microw. Millim. Wave Tech. (ICMMT)*, vol. 2, 2016, pp. 573–575.

[55] C. Yu *et al.*, "Full-angle digital predistortion of 5G millimeter-wave massive MIMO transmitters," *IEEE Trans. Microw. Theory Techn.*, vol. 67, no. 7, pp. 2847–2860, 2019.

[56] X. Liu, *et al.*, "Beam-oriented digital predistortion for 5G massive MIMO hybrid beamforming transmitters," *IEEE Trans. Microw. Theory Techn.*, vol. 66, no. 7, pp. 3419–3432, 2018.

[57] S. Lee *et al.*, "Digital predistortion for power amplifiers in hybrid MIMO systems with antenna subarrays," in *Proc. IEEE 81st Veh. Tech. Conf. (VTC)*, 2015, pp. 1–5.

[58] M. Abdelaziz, L. Anttila, A. Brihuega, F. Tufvesson, and M. Valkama, "Digital predistortion for hybrid MIMO transmitters," *IEEE J. Selec. Topic on Signal Process*, vol. 12, no. 3, pp. 445–454, 2018.

[59] E. Ng, A. B. Ayed, P. Mitran, and S. Boumaiza, "Single-input single-output digital predistortion of multi-user RF beamforming arrays," in *IEEE MTT-S Int. Microw. Symp. (IMS)*, June 2019, pp. 472–475.

[60] C. Fager, K. Hausmair, T. Eriksson, and K. Buisman, "Analysis of thermal effects in active antenna array transmitters using a combined em/circuit/thermal simulation technique," in *2015 Integrated Nonlinear Microwave and Millimetre-wave Circuits Workshop (INMMiC)*, 2015, pp. 1–3.

[61] E. Baptista, K. Buisman, J. C. Vaz, and C. Fager, "Analysis of thermal coupling effects in integrated MIMO transmitters," in *2017 IEEE MTT-S International Microwave Symposium (IMS)*, 2017, pp. 75–78.

[62] Y. Aslan, J. Puskely, J. H. J. Janssen, M. Geurts, A. Roederer, and A. Yarovoy, "Thermal-aware synthesis of 5G base station antenna arrays: An overview and a sparsity-based approach," *IEEE Access*, vol. 6, pp. 58 868–58 882, 2018.